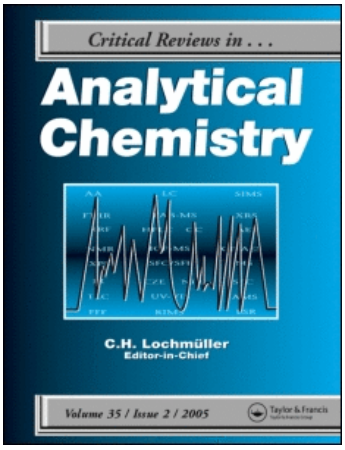

Critical Reviews in Analytical Chemistry
Publication details, including instructions for authors and subscription information:
http://www.informaworld.com/smpp/title~content=t713400837

Ion Mobility Spectrometry in Analytical Chemistry

Robert H. St. Louis[a]; Herbert H. Hill Jr.[b]; Gary Alan Eiceman[c]
[a] Advanced Research Chemist at Tennessee Eastman Kodak, Kingsport, TN [b] Department of Chemistry, Washington State University, Pullman [c] Department of Chemistry New Mexico, State University Las Cruces, New Mexico

To cite this Article Louis, Robert H. St. , Hill Jr., Herbert H. and Eiceman, Gary Alan(1990) 'Ion Mobility Spectrometry in Analytical Chemistry', Critical Reviews in Analytical Chemistry, 21: 5, 321 — 355
To link to this Article: DOI: 10.1080/10408349008050848
URL: http://dx.doi.org/10.1080/10408349008050848

Ion Mobility Spectrometry in Analytical Chemistry

Robert H. St. Louis and Herbert H. Hill, Jr.

Referee: Gary Alan Eiceman, Ph.D.
Department of Chemistry
New Mexico State University
Las Cruces, New Mexico

ABSTRACT

Recent literature relevant to the role of ion mobility spectrometry (IMS) in analytical chemistry is discussed. Included are sections dealing with instrumentation, spectral collection techniques, the theory of ion mobility in gases, and the dynamics of atmospheric pressure ionization. The pros and cons of radioactive ionization, photoionization, laser ionization, surface ionization, and electrofied spray ionization are considered. Analytical applications are separated into the use of IMS as a stand-alone spectrometer, and the use of IMS as a detector following gas, liquid, and supercritical fluid chromatography.

I. INTRODUCTION

Although the potential application of ion mobility spectrometry (IMS) to analytical chemistry has been known for over 20 years, only recently have advances in technology, design, and commercialization enabled the implementation of this simple and sensitive method of analysis for the detection of trace quantities of organic compounds. Over the past decade, IMS has evolved into an inexpensive and powerful technique for the detection of many trace compounds after chromatographic separation and direct monitoring of specific compound classes such as chemical warfare agents and drugs of abuse. The intent of this review is to provide the reader with an overview of response mechanisms, instrumentation, and applications of IMS with a critical look at some of the current limitations and future possibilities of the method for analytical chemistry.

IMS is a gas phase electrophoretic analytical technique, first introduced in 1970 under the name plasma chromatography.[1,2] Original plasma chromatographs used ^{63}Ni radioactive sources to ionize organic sample vapors through a series of ion/molecule reactions. Interest in the technique was aroused by the excellent detection limits, the speed of response, and its applicability to numerous organic functionalities. Early papers were written on the detection of alcohols,[3] alkyl halides,[4] halogenated aromatics,[5] alkanes,[6] nitrosamines,[7] alkyl acetates,[8] alkyl amines,[9] and nitroaromatics.[10] Limits of detection in the parts-per-trillion or picogram range were reported.

Almost since its inception, IMS has been suggested as a tuneably selective detector for gas chromatography.[11] High resolution capillary gas chromatography with ion mobility detection was first accomplished in 1982[12] following detector modifications designed to reduce sample residence times and thus preserve chromatographic separations. The applicability of IMS to detection after supercritical fluid chromatography has also been demonstrated.[13] Its potential capability of providing responses when using ionizable supercritical fluid modifiers is especially valuable.[14]

Since 1980, several additional methods have been introduced as ionization sources for IMS. These include photoionization,[15] laser multiphoton ionization,[16] electrified spray ionization,[17] and surface ionization.[18] Ammonia,[19] acetone,[20] and chloride[21] reactant ions have provided increased specificity of ionization in ^{63}Ni sources.

Samples of low volatility have been successfully analyzed using thermal desorption[22] and laser desorption[23] sample introduction techniques. A membrane inlet system has eliminated some difficulties associated with direct sampling of ambient air.[24] A continuous standard addition methodology has also been devised[25] for ambient measurement of toxic vapors in industrial environments. Several portable field instruments[26] have been devised for hazardous waste and chemical warfare monitoring. A sophisticated second derivative algorithm has been devised for separation of overlapping peaks.[27] Rapid, low noise, spectral collection is now possible using signal-averaged or Fourier transform techniques.[28]

This review discusses these subjects in some detail in an attempt to identify the role of IMS in analytical chemistry. As with any analytical technique, its suitability for a particular application must be approached on an individual basis. Factors to be considered include detection limits, response time, matrix interference, cost, setup time, portability, etc. A comprehensive discussion of IMS with ^{63}Ni ionization has been published.[29] An additional recent review of IMS instrumentation is also highly informative.[30]

II. INSTRUMENTATION

A. Basic Components

The basic components of an ion mobility spectrometer consist of: (1) a sample inlet system, (2) an ionizer, (3) a reaction region, (4) an ion gate or gates, (5) a drift region, and (6) an

R. H. St. Louis received his B.A. from the University of Washington, Seattle; his Ph.D. was earned at Washington State University, Pullman. Dr. St. Louis is currently an Advanced Research Chemist at Tennessee Eastman Kodak, Kingsport, TN. **H. H. Hill, Jr.** received his B.S. from Rhodes College, Memphis, Tennessee; his M.S. was earned at the University of Missouri, Columbia; a Ph.D. was granted by Dalhousie University, Halifax, Nova Scotia, Canada. Dr. Hill is a Professor, Department of Chemistry, Washington State University, Pullman.

ion collector. Figures 1 and 2 illustrate these components in a conventional bidirectional gas flow, ^{63}Ni ionization, stacked ring design IMS. Gas to be analyzed is introduced into the reaction region by an inert carrier gas. Sample product ions are formed and directed toward the drift region by an applied electric field. A narrow pulse of ions is injected into the drift region using an ion shutter grid (see Figures 1 and 2). In the drift region, ions of different identities are separated based upon their charge, mass, and size. The analytical signal is obtained when ions strike a conducting flat plate (Faraday cup), and the resulting current is amplified with a fast electrometer.

Ancillary equipment needed to provide a functioning IMS include (1) a high voltage power supply to create the electric field in the drift tube, (2) a shutter controller, (3) an external source of clean carrier and drift gases, (4) temperature control instrumentation, (5) a fast electrometer, and (6) data collection apparatus including computer, signal averager, and printer.

Ion identifications can be obtained by coupling the IMS to a quadrupole mass spectrometer via a pinhole aperture in the ion collector plate. This opening is illustrated in Figure 1.

Attempts to couple gas chromatography to a bidirectional gas flow IMS were only marginally successful. Excessive detector residence times were noted that sacrificed chromatographic resolution. Figure 3 illustrates a unidirectional flow IMS designed to alleviate this difficulty. In this design, chromatographic effluent is efficiently swept through the ionizer and out of the detector with residence times of seconds. No sensitivity losses were noted. More detailed discussion of IMS detectors for chromatography is provided later in a chromatography section in this review.

In order to reduce the complexity and expense of the stacked ring designs, the conductive inlaid tube was designed.[31] The conductive inlaid tube is composed of a ceramic material (macor or alumina) coated internally with resistive ink to provide a linear resistance along the length of the tube. This instrument is illustrated in Figure 4. Comparative studies between this tube and one of a stacked ring design of similar dimensions revealed no significant differences in sensitivity, resolution, or total ion current. Its primary advantage would seem to be its simplicity, providing greater ruggedness and stability for use in a portable device.

B. Sample Inlets

Several methods have been described for introducing sample vapors into the ionization region of an IMS. These include sample wire probe,[32] syringe injection,[33] exponential dilution flask,[10] permeation tubes,[34] diffusion tubes,[35] thermal desorption ovens,[22,36] laser desorption,[37] and suction of ambient air into the instrument either directly or through a membrane in-

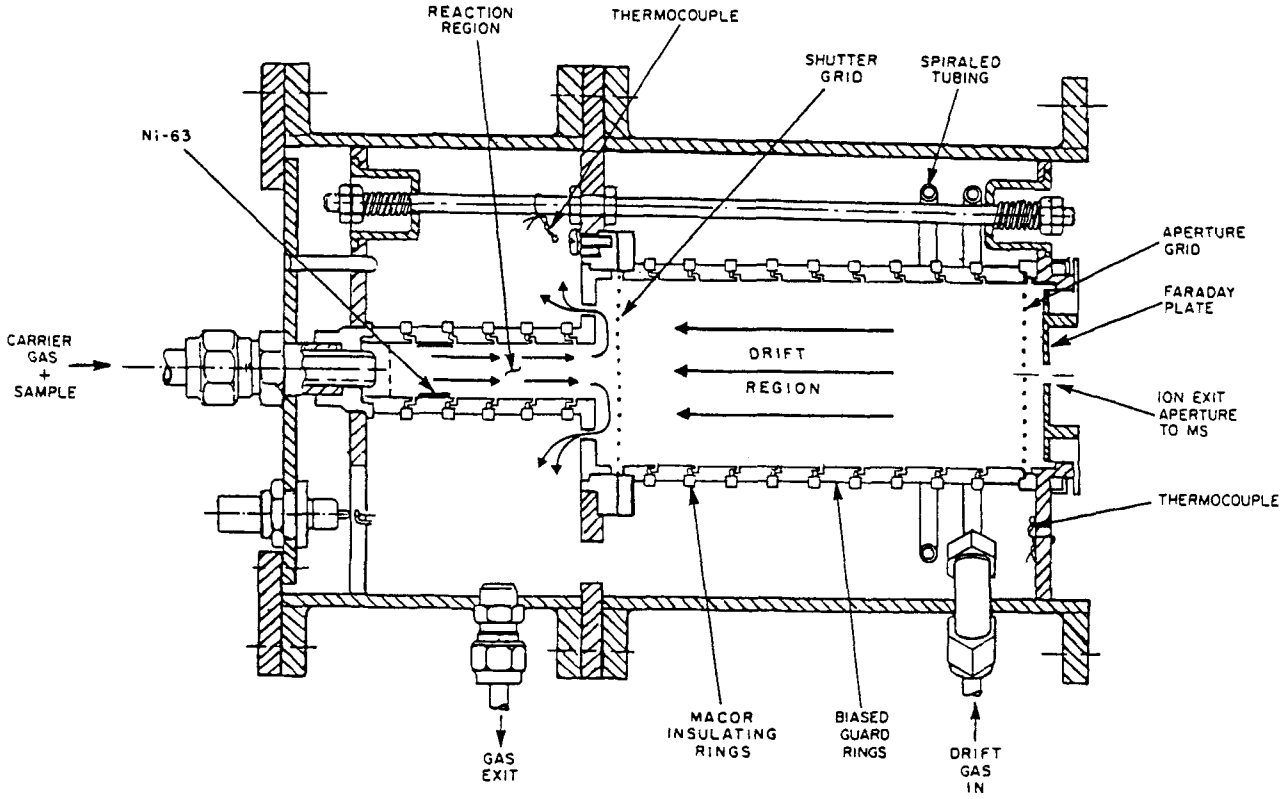

FIGURE 1. Detailed diagram of an ion mobility spectrometer. Note the opposing gas flows in the reaction and drift regions. (Reprinted from Spangler, G. E. and Carrico, J. P., *Int. J. Mass Spectrom. Ion Phys.*, 52, 267, 1983. With permission.)

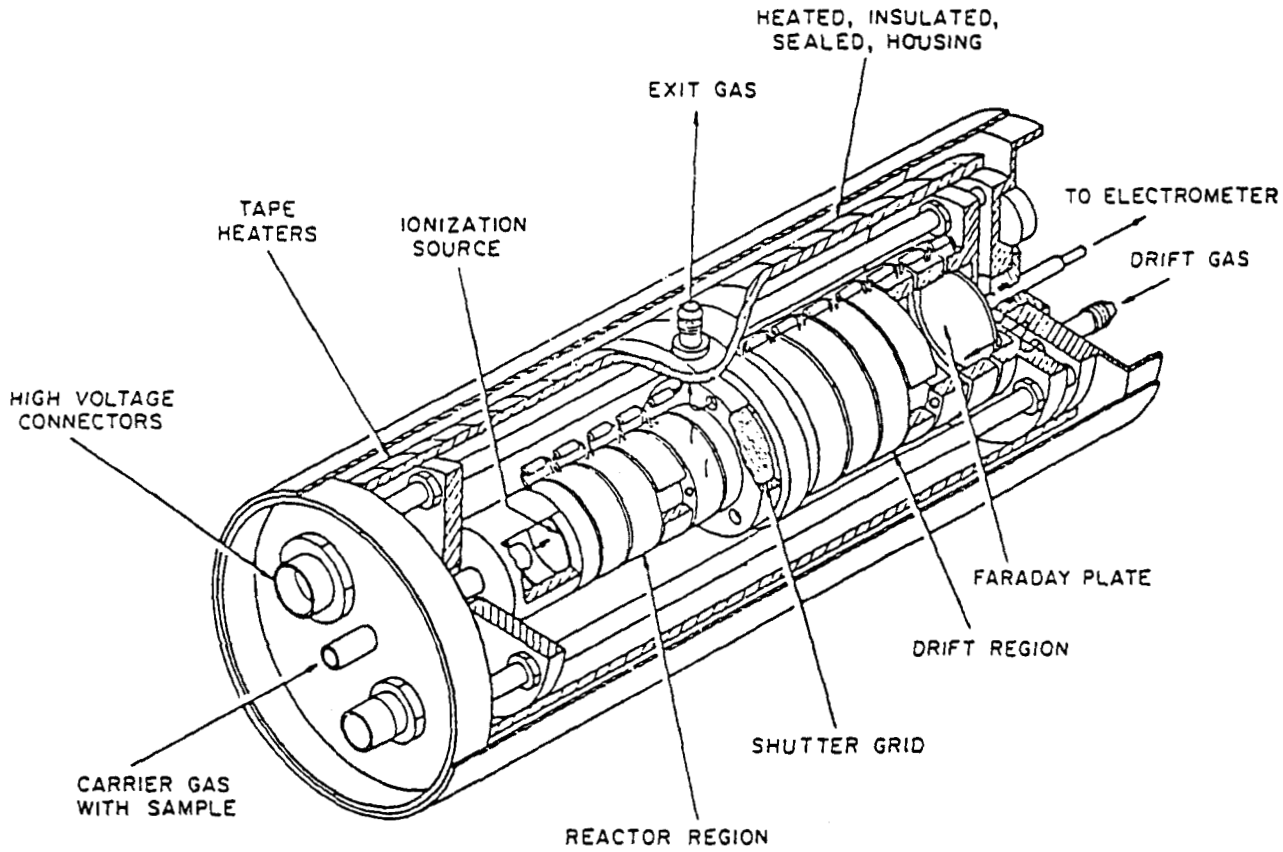

FIGURE 2. Three-dimensional drawing of conventional ^{63}Ni ionization, bidirectional gas flow, stacked ring design ion mobility spectrometer. (Reprinted from Spangler, G. E., Campbell, D. N., Vora, K. N., and Carrico, J. P., *ISA Trans.*, 23, 17, 1984. With permission.)

let.[24,38] Chromatography, which could be considered as merely an inlet, is discussed separately.

The thermal desorption oven technique has been used for analysis of surface contamination of electronic components,[22] and for sampling for residue from drugs of abuse.[36] In the first case, the surface sample was placed in a temperature-programmable inlet oven. Flowing through the oven is the carrier gas of the IMS, so that as the surface sample is heated up, sample vapors are introduced directly into the ionization region. In the drug-sampling scenario, persons suspected of handling drugs are sampled on their palms, fingers, injection sites, and/or nostrils for residue. The sampling device was a small nickel tube (6 × 0.3 cm) containing a fine mesh platinum filter. This probe was connected to a battery-powered, handheld pump. During sampling, the probe was applied to the skin surface, and drug particulates are sucked into the tube and adsorbed on the filter. The tube was then inserted into the heated inlet of an IMS. Volatile substances evaporate immediately and are flushed with the carrier gas into the ionization region of the instrument.

Laser desorption has been used to volatilize thermally labile explosive materials for subsequent analysis by ion mobility/mass spectrometry measurements.[37] The laser desorption was performed at relatively low power ($<10^7$ W/cm^2) so that mainly neutrals were produced, which were subsequently ionized by ^{63}Ni-induced ion-molecule reactions at atmospheric pressure. A thin layer of sample paste was applied to the end of a ceramic rod which was then inserted into an IMS. The sample was irradiated with the 532-nm second harmonic of a Nd:YAG laser, at a laser power sufficient to desorb the sample in 15 s to several minutes. This slow desorption was used, so as not to saturate the ^{63}Ni reactant ions. A minimum detectable limit of 280 pg trinitrotoluene (TNT) was obtained.

Direct sampling of ambient air is complicated by changes in the identity of reactant ions when introducing laboratory air directly into an IMS. Ambient water and ammonia cause highly clustered ammonium reactant ions of high proton affinity to be formed in the positive ion spectrum. Highly clustered nitrate and chloride reactant ions of high electron affinity were seen in the negative ion spectrum.[24] This clustering places limitations on the ability of IMS to analyze sample constituents of low proton or electron affinities and introduces other ion/molecule reactions, e.g., nucleophilic attachment reactions for ammonia. A membrane can be used on an IMS inlet to sample ambient air and discriminate between organic vapors and water/ammonia, thus minimizing complications in ion creation and mobility analysis caused by clustering reactions.

A schematic of a single stage membrane inlet system is

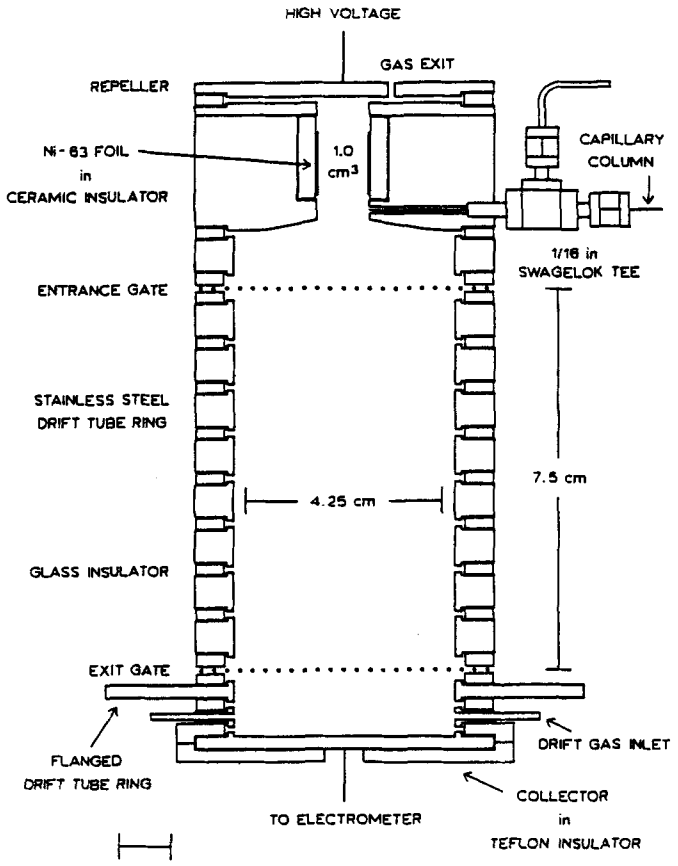

FIGURE 3. Unidirectional gas flow ion mobility spectrometer used as a detector after capillary gas chromatography. (Reprinted from Baim, M. A. and Hill, H. H., Jr., *Anal. Chem.*, 54, 38, 1982. With permission.)

illustrated in Figure 5. The ambient air containing the sample is drawn across the external surface of the membrane by a suction pump. The sample permeates the membrane in accordance with the following equation.

$$P_I = \frac{A_m P_r P P_x}{F_c H + P_r A_m P} \quad (1)$$

where P_I is the partial pressure of the sample interior to the membrane, P_x is the partial pressure external to the membrane, P_r is the permeability coefficient of the membrane, and P is atmospheric pressure. A_m is the cross-sectional area of the membrane, and H is the membrane thickness. F_c is the carrier gas flow rate which carries the sample internal to the membrane into the IMS. Permeability coefficients for various membranes have been studied.[39-41] A dimethylsilicone membrane (25 μm thick) has been found to significantly reduce effects from ambient air on both positive and negative reactant ions.[24] Figures 6 through 8 are positive reactant ion spectra using purified air, unfiltered laboratory air, and laboratory air filtered with a dimethylsilicone membrane, respectively. Total ion mass spectra associated with each ion mobility spectra identify the contaminated spectra of Figure 7 to be primarily due to water-ammonium ion clusters. These clusters are largely eliminated when using the dimethylsilicone membrane.

IMS with a dimethylsilicone membrane has been used to detect 2,4,6-trinitrotoluene vapors in ambient air. A limit of detection of approximately 500 ppt was reported.[42] This represents a loss in sensitivity of greater than an order of magnitude from earlier reported TNT detection limits.[10]

C. Ion Gates

Two basic approaches have been used to control ions. They both involve creating an electric field between fine wires strung across the drift tube. The voltages used to create the gate field are electrically referenced to the gate's position in the drift field. The gate is opened by removing the gate field, allowing the gate wires to assume the potential of their location in the drift field.

The two approaches differ in the positioning of the fine wires. In the Tyndall gate,[43] two independent grids composed of finely spaced wires were separated by 1 mm and placed across the drift tube. The gate was closed by applying a voltage across the two grids which reversed the drift field in the vicinity of the gate. This reversed field directed the ions to the gate wires of the first grid where they were neutralized.

In the Bradbury and Nielsen gate,[44] the ions were passed in a single plane of the drift field. The gate consists of a single grid of finely spaced wires, alternate wires being biased + and − the gates reference voltage, creating an orthogonal gate field to the drift field. This orthogonal field is some three times the drift field, directing the ions into the wires where they are nuetralized.

D. Drift Rings

Ions are directed down the drift tube toward the collector by an electric field created by the voltage differential between a repeller plate and the grounded collector. This field is maintained and guarded from stray fields by enclosing the drift space within a cylindrical tube composed of identical equally spaced stainless steel guard rings. Voltages suitable to the rings' position within the field are applied by tapping a string of resistors, connected in series down the length of the tube.

Uniformity of the drift field in such a system has been previously studied.[32] It was found that field uniformity is primarily a function of c/h, where c is the radius of the guard ring, and h is the distance between the centers of the gaps of successive rings. Expressed algebraically, h = 2b + 2f, where 2b equals the height of the guard ring and 2f is the gap between the rings. Figure 9 displays the radial position, r/c, where the maximum distortion in the electric field, ΔE, is 1% for different values of c/h. Field uniformity is improved by increasing the value of c/h. This can be done by increasing c, the guard ring radius, or by decreasing h by using a greater number of thinner rings separated by smaller gaps. The dotted line in Figure 9, relates

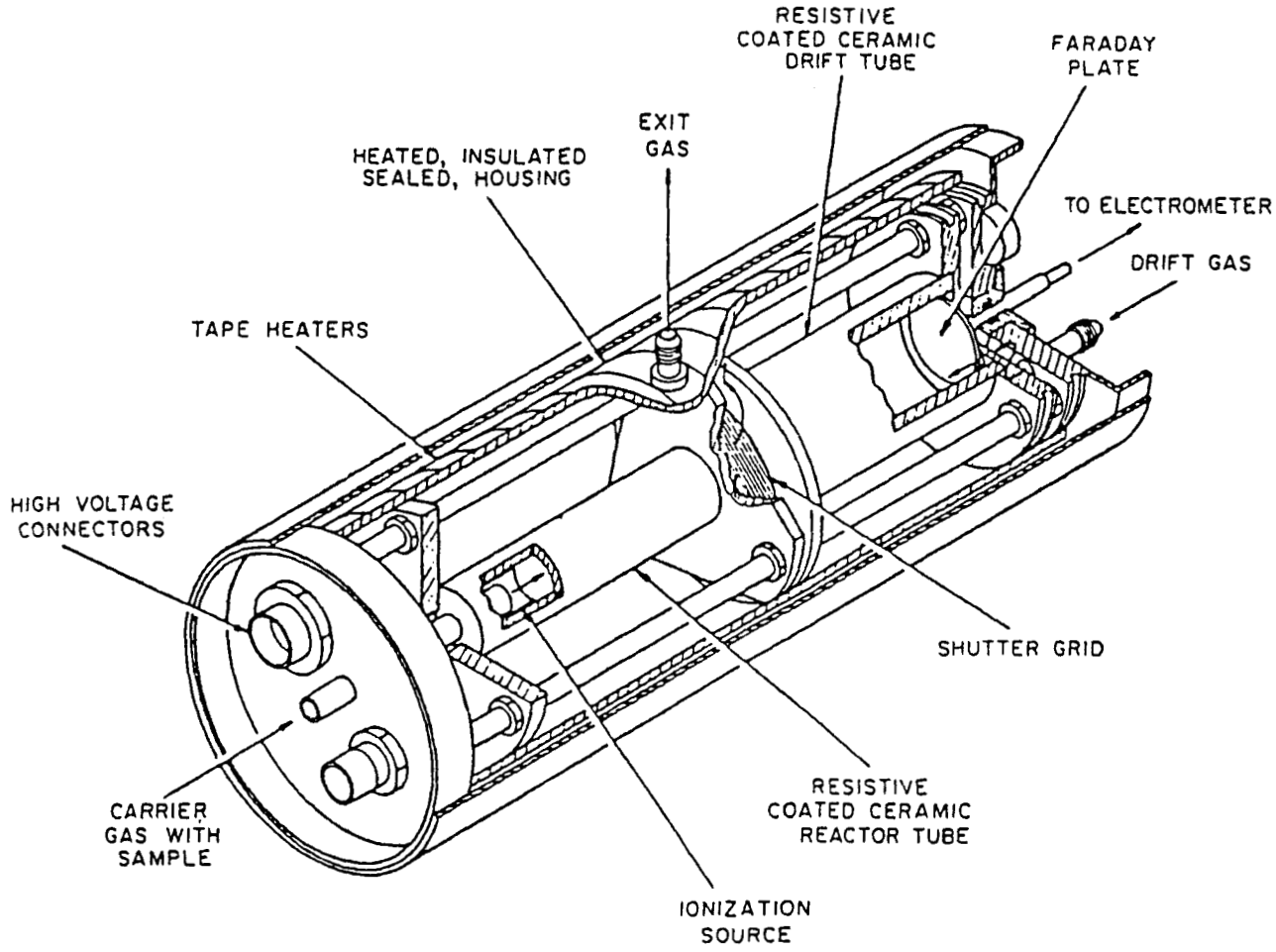

FIGURE 4. Ceramic tube design ion mobility spectrometer. A linear resistance is created along the drift tube by an internal coating of resistive ink. (Reprinted from Spangler, G. E., Campbell, D. N., Vora, K. N., and Carrico, J. P., *ISA Trans.*, 23, 17, 1984. With permission.)

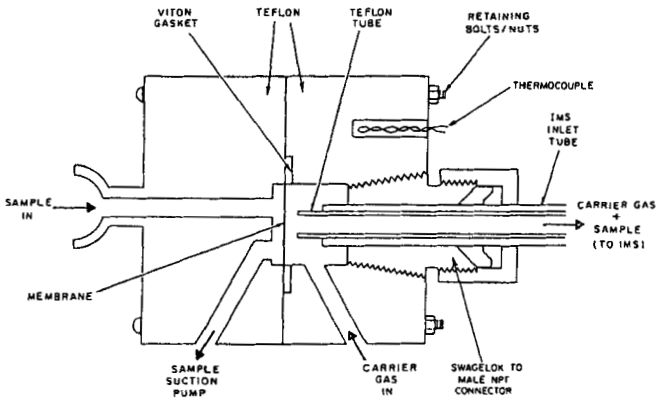

FIGURE 5. Schematic of membrane inlet system. (Reprinted from Spangler, G. E., Campbell, D. N., Vora, K. N., and Carrico, J. P., *ISA Trans.*, 23, 17, 1984. With permission.)

to dimensions of a commercial ion mobility spectrometer. This instrument had a c/h value of 2.12; 1% error occurred at r/c = 0.58. Ions introduced from the 1.41 cm diameter of the reaction region into the 4.25 cm diameter of the drift region thus saw less than 1% distortion of the electric field. A detailed discussion of the electrical field near the ion gate has also been published.[45] This same report touches upon problems of imperfect gating, including static leakage, gate depletion, and dynamic leakage.[46]

E. Aperture Grid

In order to maintain spectral resolution in single-scan or signal-averaged spectral collection, an aperture grid must be placed approximately 1 mm prior to the ion collector. The aperture grid is designed similarly to a Bradbery/Nielsen ion gate, consisting of thin, finely spaced parallel wires, or it can be a fine mesh. An appropriate voltage is applied to the wires or mesh in order to maintain the drift field near the collector. As an example, for a drift field of +300 V/cm, the aperture grid 1 mm from the collector would be held at +30V. The function of the aperture grid is to capacitively decouple the collector from the approaching ion swarm. Without the aperture grid, the ion swarm is coulombicly felt by the collector several

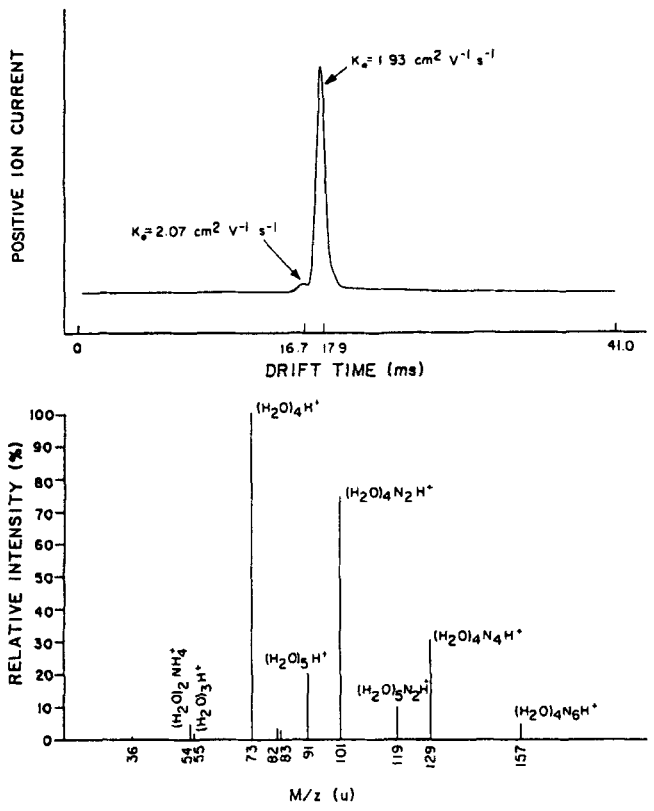

FIGURE 6. Positive reactant ions for IMS/MS without a membrane inlet system using purified air for carrier and drift gases. (Reprinted from Spangler, G. E. and Carrico, J. P., *Int. J. Mass Spectrom. Ion Phys.*, 52, 267, 1983. With permission.)

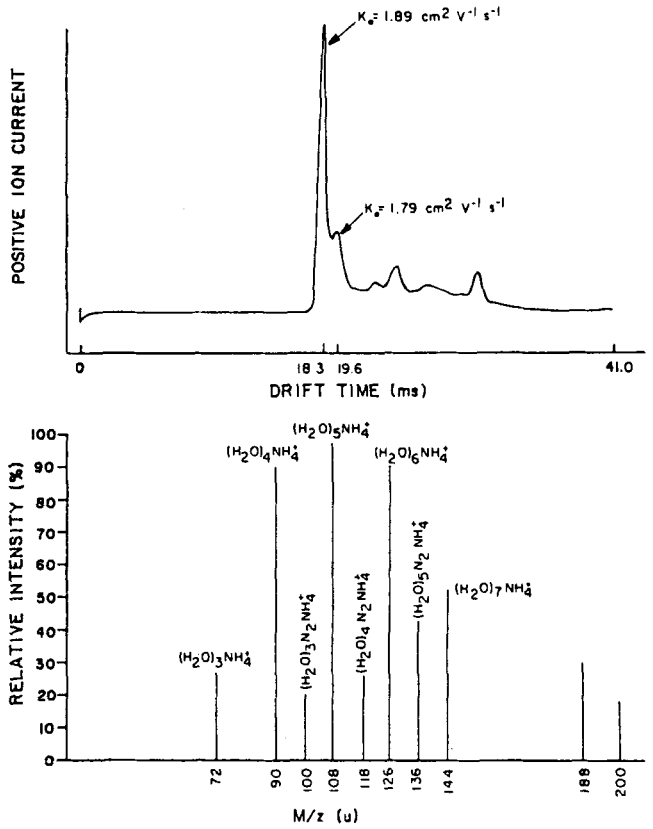

FIGURE 7. Positive reactant ions for IMS/MS without a membrane inlet system using unfiltered laboratory air for carrier gas and purified air for drift gas. (Reprinted from Spangler, G. E. and Carrico, J. P., *Int. J. Mass Spectrom. Ion Phys.*, 52, 267, 1983. With permission.)

millimeters prior to its actual arrival. The result is a broadening of the ion peaks and a loss in spectral resolution. Decreases of total ion current and sensitivity of up to 2.5 times have been measured with the aperture grid installed,[46] probably due to neutralization of ions on the fine wires or mesh. Microphonics of the aperture grid to the detector plate contribute major portions of noise to the IMS signal.[47] An aperture grid is not necessary when using Fourier transform spectral collection (as is discussed in the section entitled Spectral Collection).

III. ION MOBILITY IN GASES

In IMS, ions are separated and detected based upon the differing velocities attained when accelerated down an electric field against a counterflowing neutral drift gas. Mason et al. have published several reviews of ion mobility in gases.[48-50] The average velocity of the ion, v_d, is determined by the number of collisions that the ion makes with the molecules of the drift gas and, at low field strengths, is directly proportional to the electric field, E.

$$v_d = KE \qquad (2)$$

where v_d is the velocity of the ion (cm/s), E is the electric field (V/cm), and K is the mobility of the ion (cm^2/V-s). The mobility, K, is a combined property of the ion and the drift gas.

$$K = 3/16\ q/N\ (2\pi/\mu kT)^{1/2}\ (1 + \alpha)/\Omega_D \qquad (3)$$

This is known as the Mason-Schamp mobility equation; q is equal to ze, where z is the charge on the ion and e is the unit electronic charge (1.602×10^{-19} C). N is the number density of the drift gas (molecules/cm). $\mu = mM/(m + M)$, the reduced mass of a colliding ion-drift gas pair, where m is the mass of the ion, and M is the mass of a neutral drift gas molecule. k is Boltzman's constant (1.381×10^{-23} J/K), and T is the temperature in degrees Kelvin. α is a correction term which is less than 0.02 when $m > M$, generally the situation in organic analysis using the most common drift gases, N_2 or air. Ω_D is the ion-neutral cross section which is derived through a series of integrations averaging the ion-neutral collisions over all possible scattering angles and energies. For spherically symmetric forces, the integrations are as follows

$$\Omega_D\ (T) = 1/2\ (kT)^{-3} \int_0^\infty Q_D\ (\epsilon)\ \exp\ (-\epsilon/kT)\epsilon^2\ d\epsilon \qquad (4)$$

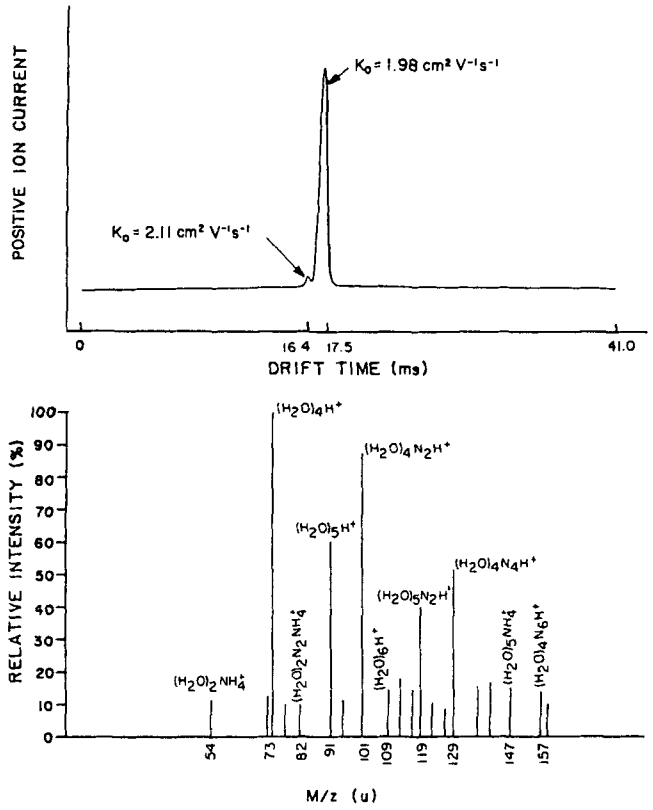

FIGURE 8. Positive reactant ions for IMS/MS with a dimethylsilicone membrane inlet system using purified air for carrier and drift gases and unfiltered laboratory air (72 to 100% relative humidity) for sample gas. (Reprinted from Spangler, G. E. and Carrico, J. P., *Int. J. Mass Spectrom. Ion Phys.*, 52, 267, 1983. With permission.)

$$Q_D(\epsilon) = 2\pi \int_0^{\pi} (1-\cos\theta)\, s(\theta,\epsilon)\sin\theta d\theta \qquad (5)$$

ϵ is the relative kinetic energy of a collision, and $s(\theta,\epsilon)$ is the differential cross section for scattering through an angle θ when the collision energy is ϵ. For rigid sphere collisions, integrating analytically yields, $\Omega_D = \pi d^2$, where d is the sum of the ion and drift gas radii. From Equation 3 for the mobility, K, it can be seen that what is essentially measured in the IMS experiment is the $q/\mu^{1/2}\Omega_D$. For small atomic ions in the same neutral drift gas, mobility is largely controlled by the reduced mass. For heavy ions, μ is essentially equal to M, the mass of the neutral drift gas molecule, thus the distinguishing property upon which large ions are separated is ionic size through the Ω_D term. For those ions falling between these extremes, which includes most of the polyatomic ions for which ion mobility spectra have been reported, mobility is a function of both mass and shape. Analysis of mass-mobility correlations[51] revealed a standard error of ±20% for structurally unrelated compounds, but only ±2% for a series of similar polynuclear hydrocarbons. Figure 10 demonstrate mass-mobility correlations for phosphorus esters, monohalogenated benzenes, halogenated nitrobenzenes,

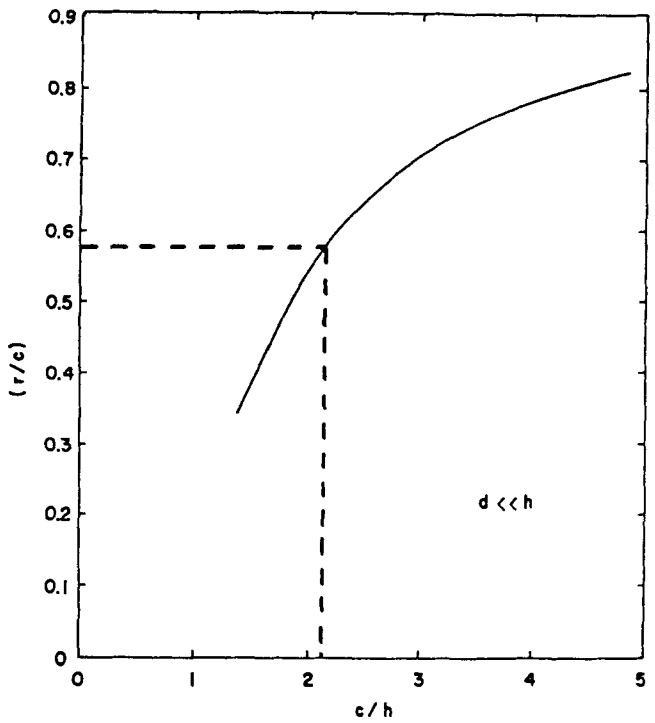

FIGURE 9. Solid line indicates the fractional radial position at which the maximum distortion of the electric field equals 1%. Details in text, section entitled Drift Rings. (Reprinted from Carr, T. W., *Plasma Chromatography*, Plenum Press, New York, 1984. With permission.)

aliphatic n-nitrosamines, oxygenated compounds, 2-alkyl, and normal alkanes.[52] Clearly, mass measurement from an ion mobility experiment is a very approximate process.

The primary reason for the approximate nature of mass-mobility correlation curves is the effect of size and shape of the molecule. As described in the Mason-Schamp equation, ions with larger collisional cross sections travel slower. In early mobility work where mobilities of inorganic ions were measured, effects of size and shape were minimal relative to those of mass. Differences in collisional cross sections of organic ions and their effect on mobilities are best observed for the ion mobility separations of isomers. Karasek and Kane[53] demonstrated isomer separation by IMS using 4-bromonitrobenzene and 3-bromonitrobenzene. Other examples of isomer separation were noted in the early literature,[54,55] but the first systematic study of the subject was reported by Hagen, in which he concluded that meta-substituted positional isomers are generally larger than the para- and ortho-isomers.[56]

More recently, Karpas et al. have empirically investigated the effects of size and shape on mobility. Using IMS coupled with mass spectrometry, they were able to show that the soft ionization process of the ^{63}Ni source did not usually lead to isomerization of the compounds, and that the separate identities of isomeric structures were retained after ionization.[57] They also demonstrated that not only structure, but also charge distribution was important for ion mobility.[58] In an extensive

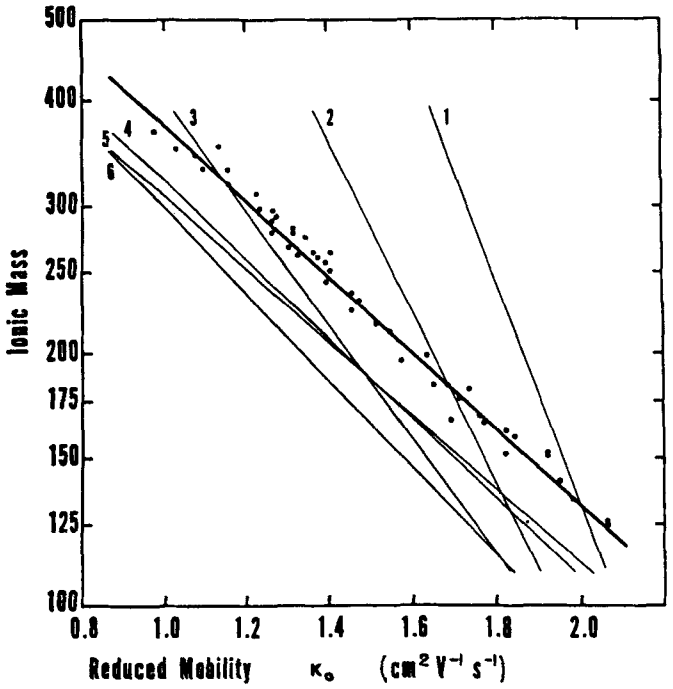

FIGURE 10. Ion mass vs. reduced mobility. Dots indicate a group of phosphorus esters. Lines indicate (1) monohalogenated benzenes, (2) halogenated nitrobenzenes, (3) aliphatic n-nitrosamines, (4) oxygenated compounds, (5) 2-alkyl alkanes, and (6) normal alkanes. (Reprinted from Carr, T. W., *Plasma Chromatography*, Plenum Press, New York, 1984. With permission.)

investigation of amines, Karpas concluded that structural effects increased ion mobility in the following order:[59]

primary<secondary<tertiary
linear<branched
normal<secondary
aliphatic<aromatic
amine<amide

The mobility equation also reveals an inverse relationship between K and N, the number density of the drift gas. This is as expected since it is collisions with the drift gas that ultimately limits the ionic velocity. Increased number density, N, yields increased number of collisions, decreased ionic velocity, v_d, and decreased mobility, K. Standard procedure is to measure the drift time, t_d, of an ion through a specified drift length, l_d, under a known electric field, E.

$$v_d = l_d/t_d = KE \quad (6)$$

$$K = l_d/t_dE \quad (7)$$

This mobility value is then corrected to standard gas density, 2.687×10^{19} molecules/cm, corresponding to 273 degrees Kelvin and 760 torr, and reported as the reduced mobility, K_o.

$$K_o = K\,(P/760)\,(273/T) \quad (8)$$

This is a simple ideal gas law conversion, correcting for changes in the number density of the drift gas at different pressures and temperatures. A comprehensive table of reduced mobility values, reported in the open literature from 1970 to 1984, has been previously compiled.[60] This table is probably best used as an identifier of potential interferents, rather than for qualitative identification. Interinstrument comparisons have revealed variations in K_o, potentially due to several factors, including (1) imprecise determinations of the electric field, (2) imprecise temperature measurements of the drift space, (3) temperature gradients, (4) pressure fluctuations, especially when the drift gas flow rate is pump controlled, and (5) variable water content of the drift gas, affecting primarily the water content of the clustered reactant ions. Additionally, much of the data was obtained using sample introduction techniques that overloaded the system and did not guarantee sample purity. Under these saturated conditions, multiple peaks due to contaminants in the sample, dimer formation, and ion-molecule reactions in the drift space are not uncommon. Samples introduced via high-resolution capillary gas and supercritical fluid chromatography in low and subnanogram amounts have rarely exhibited multiple peaks.

In addition to the temperature dependence of the number density, N, the mobility equation shows a variation in K with $T^{-1/2}$. The ion-neutral cross section, Ω_D, for most systems varies as T^{-2}, thus K_o is approximately independent of T,[50] as has been found experimentally for laser and ^{63}Ni-produced product ions for temperatures ranging from 85 to 220°C.[61,62]

Other work with a ^{63}Ni ionization source[63] has demonstrated increasing K_o values for reactant ions as the temperature increased from 150 to 300°C. These variations probably reflect decreased H_2O content of the hydrated reactant ions at higher temperatures.

K_o values have also been compared using different drift gases, including N_2, air, argon, argon-methane, and CO_2.[64] The reduced mobility was found generally to change as a function of the polarizability, α, of the drift gas. Mobility in IMS is essentially determined by the number of collisions between the analyte product ions and the neutral drift gas. For drift gases of high polarizability, the attractive forces between the product ion and the induced dipole moment of the drift gas would be increased, leading to a greater number of collisions and consequently a lowered mobility. This was found to be true upon switching from N_2 to argon drift gas. The significantly lower mobilities in CO_2 could not fully be accounted for by polarizability differences, and clustering of CO_2 around the product ions was suggested.[13,64]

As previously stated, Equation 2, $v_d = KE$, is true only at low field strengths, the definition of which was derived by Wannier[65] and Mason.[50] Their calculations found that low field behavior is exhibited when:

$$E/N < \frac{3\pi d^2}{z}\left(\frac{kT}{e}\right)\left(\frac{m}{m+M}\right)^{1/2} \quad (9)$$

Using Cl^- as the product ion, m, and 4.0×10^{-8} cm as a representative d for a singly charged ion in nitrogen drift gas,[48] the right hand side of Equation 9 equals 3.12×10^{-16} V cm^2 at 150°C.[66] The number density, N, at this temperature and 700 torr is 2.09×10^{19} cm^{-3}. The electric field, consequently, must be greater than 6521 V/cm for the above equation to not hold. Commonly used electric fields in analytical applications of IMS are in the range of 100 to 350 V/cm, very safely in the range for which the drift velocity, v_d, is directly proportional to the electric field, E, and the mobility, K, is independent of the electric field.

IV. RESOLUTION

Resolution, R, measures the ability of an instrument to distinguish two closely spaced peaks from a single broad peak. A practical measure of resolution in IMS[67] is

$$R = t_d/2T_{1/2} \quad (10)$$

where t_d is the drift time of the peak, and $T_{1/2}$ is its temporal width at half height. Experimentally, a number of factors potentially contribute to $T_{1/2}$ and to peak shape. These include (1) initial pulse width and shape, (2) diffusional broadening, (3) Coulombic repulsion, (4) capacitive coupling between approaching ions and the collector, (5) field gradients, (6) temperature gradients, (7) gate depletion/dynamic leakage, (8) pressure fluctuations, and (9) ion-molecule reactions in the drift space. Current work in the authors' laboratory[46] addresses these issues; the general discussion that follows describes the approach being taken to separate the measured width at half height, $T_{1/2}$, into components of initial pulse width, to broadening due to diffusion, $t_{1/2}$, and broadening due to other factors, t_x.

Effects due to Coulombic repulsion are generally disregarded for reasons demonstrated by the following calculation. Reactant ion current in the system used was approximately 6×10^{-10} A, which corresponds to 6×10^{-13} C/ms. Dividing by Faraday's constant, 96500 C/mol, yields 6.2×10^{-18} mol of ions or approximately 4×10^6 ions reach the collector per millisecond. The drift velocity was on the order of 0.7 cm/ms, and the ion pulse diameter was about 1 cm. A 1 ms long ion pulse thus corresponds to a volume of about 0.6 cm^3. Each ion occupies about 1.5×10^{-7} cm^3, and the average distance between ions is roughly 5×10^{-3} cm. Using Coulombs law, an ion at this separation would produce an electric field of about 5×10^{-3} V/cm at its nearest neighbor. This can be compared to a drift voltage of ≈240 V/cm.

Diffusional broadening is not insignificant and has been previously investigated in some detail.[49] Imagine an infinitely thin pulse of ions being admitted through the entrance gate of a drift tube, this pulse having no ions per unit area. After a time t, the plane of ions have traveled a distance $x = v_d t$ and has changed by diffusion to a Gaussian distribution. The ion concentration at time, t, at any point, x, along the drift axis is

$$n(x,t) = \frac{n_o}{2(\pi Dt)^{1/2}} \exp -(x-x_d)^2/4Dt \quad (11)$$

where D is the diffusion coefficient of the ion, and x_d is the center of the Gaussian ion pulse. The half-height spatial width of this Gaussian[50] is

$$S_{1/2} = 4(Dt)^{1/2}(\ln 2)^{1/2} \quad (12)$$

The mobility, K, is related to the ionic diffusion coefficient, D, by the Nernst-Townsend-Einstein relation:[68]

$$K = qD/kT \quad (13)$$

Rearranging:

$$D = KkT/q \quad (14)$$

Where K is the mobility, k is Boltzmann's constant, T is the absolute temperature, and q is the charge on the ion. When t, in Equation 12, is equal to the drift time, t_d, of an ion peak, $S_{1/2}$ is the spatial half width when the center of the Gaussian distribution (Equation 11) has just reached the collector.

Recall Equation 6:

$$v_d = l_d/t_d = KE$$

Multiplying both sides by the drift time, t_d, yields:

$$Kt_d = \frac{v_d t_d}{E} = \frac{l_d}{E} = l_d^2/V \quad (15)$$

where l_d is the drift length, and $V = El_d$, the total voltage drop across the drift length. Substituting first Equation 14 and then Equation 15 into Equation 12, yields:

$$S_{1/2} = 4\left(\frac{KkTt_d}{q}\right)^{1/2}(\ln 2)^{1/2} \quad (16)$$

$$S_{1/2} = 4\left(\frac{k \cdot \ln 2}{q}\right)^{1/2}(l_d^2 T/V)^{1/2} \quad (17)$$

Note that the spatial half width, $S_{1/2}$, is independent of drift time, t_d. All ion pulses have the same spatial width when arriving at the collector. This follows from the direct relationship between mobility, K, and the diffusion coefficient, D, in Equation 13. The faster moving pulse will spread more rapidly

by diffusion; however, the faster pulse arrives at the detector sooner and consequently has less time to diffuse.

Extracting the drift length, l_d, from the square root and moving to the left side of the equation yields:

$$S_{1/2}/l_d = 4\left(\frac{k \cdot \ln 2}{q}\right)^{1/2} (T/V)^{1/2} \quad (18)$$

Inverting:

$$l_d/S_{1/2} = \frac{1}{4}\left[\frac{q}{(k \cdot \ln 2)}\right]^{1/2} (V/T)^{1/2} \quad (19)$$

For singly charged ions:

$$l_d/S_{1/2} = 32.3\ (V/T)^{1/2} \quad (20)$$

If the spatial width of the peak does not change significantly during its collection:

$$S_{1/2} = v_d t_{1/2} \quad (21)$$

Substituting Equation 21, and $l_d = v_d t_d$ into Equation 20, yields:

$$\frac{v_d t_d}{v_d t_{1/2}} = \frac{t_d}{t_{1/2}} = 32.3\ (V/T)^{1/2} \quad (22)$$

Dividing by 2 provides the resolution equation.

$$R_d = \frac{t_d}{2t_{1/2}} = 16.15\ (V/T)^{1/2} \quad (23)$$

Equation 23 is the theroretical expression for diffusion-contolled resolution. The initial pulse duration is assumed to be zero and no broadening occurs by any process except diffusion. It should be noted: (1) resolution is independent of drift time, t_d. At a specific drift voltage and temperature, the ratio of $t_d/t_{1/2}$ is equal for all single species peaks; (2) resolution depends only on the voltage across the drift space, rather than any combination of electric field and drift tube length; (3) higher voltage yields a higher resolution; (4) resolution varies as $T^{-1/2}$.

Practical experience suggests different trends than the first three noted above. Actual data[67] reveal (1) resolution increases with drift time as demonstrated in Figure 11; (2) resolution is field dependent rather than voltage dependent (Figure 12); (3) in most cases, lower voltage yields higher resolution; (4) Figure 13 reveals that there is, in fact, a linear relationship between resolution and $T^{-1/2}$.

These apparent contradictions are explained when the initial pulse width is included in the calculations. If the initial pulse had a Gaussian shape with half width, t_o, then the measured pulse width, $T^{1/2}$, would be related to the initial pulse width

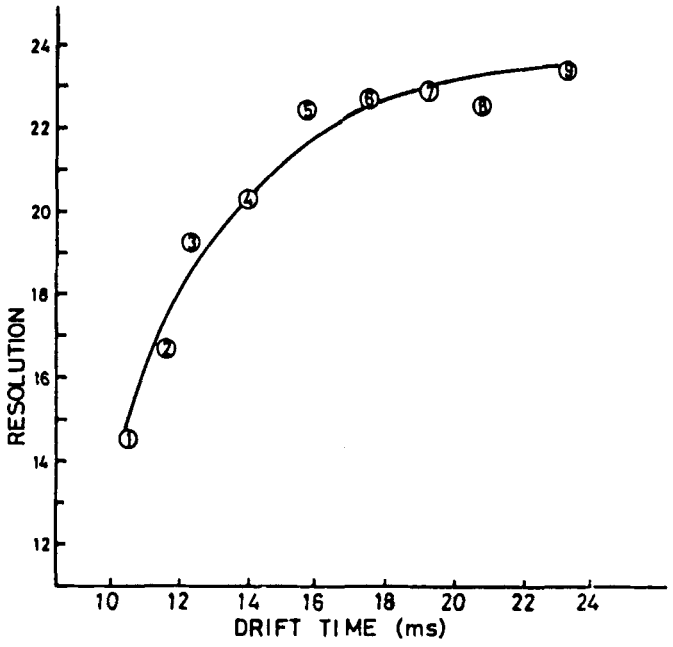

FIGURE 11. IMS resolution measured as a function of drift time at an entrance gate width of 0.2 ms. (Reprinted from Rokushika, S., Hatano, H., Baim, M. A., and Hill, H. H., Jr., *Anal. Chem.*, 57, 1902, 1985. With permission.)

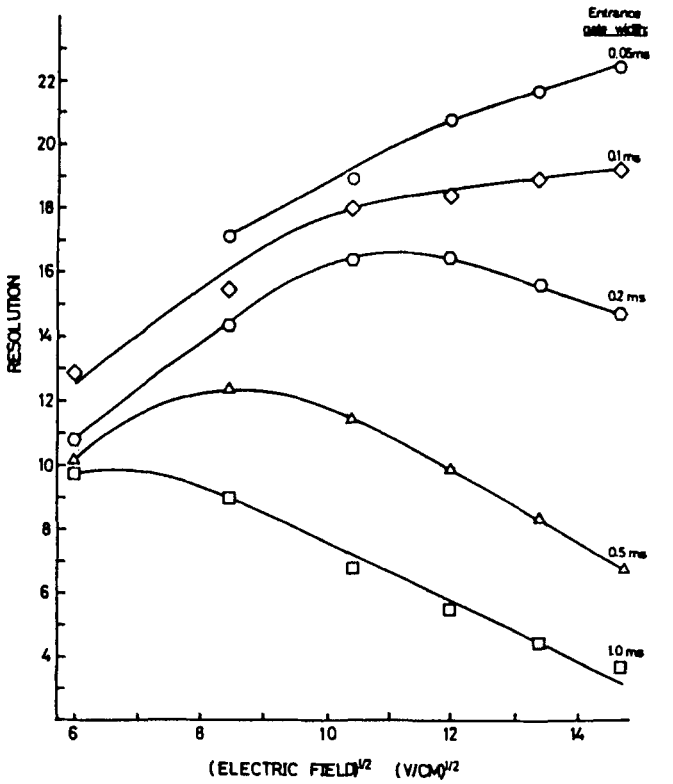

FIGURE 12. IMS resolution measured as a function of electric field at different entrance gate widths. (Reprinted from Rokushika, S., Hatano, H., Baim, M. A., and Hill, H. H., Jr., *Anal. Chem.*, 57, 1902, 1985. With permission.)

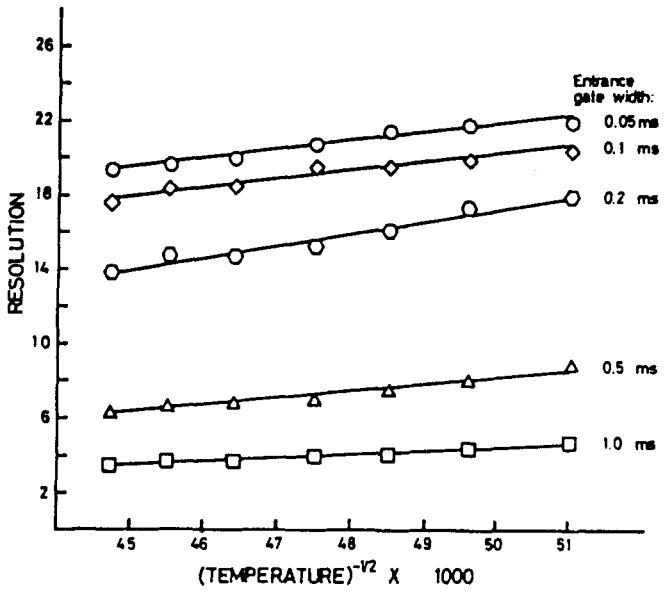

FIGURE 13. IMS resolution measured as a function of drift gas temperature at different entrance gate widths. (Reprinted from Rokushika, S., Hatano, H., Baim, M. A., and Hill, H. H., Jr., *Anal. Chem.*, 57, 1902, 1985. With permission.)

and the diffusion controlled pulse width, $t_{1/2}$, by the following relation:

$$T_{1/2}^2 = t_o^2 + t_{1/2}^2 \quad (24)$$

Solving Equation 23 for $t_{1/2}$:

$$t_{1/2} = \frac{t_d(T/V)^{1/2}}{(2)\ (16.15)} \quad (25)$$

Substituting into Equation 24:

$$T_{1/2}^2 = t_o^2 + \frac{t_d^2}{1043}\ (T/V) \quad (26)$$

If measured peak width, $T_{1/2}^2$, is plotted vs. drift time squared divided by voltage, t_d^2/V, Equation 26 should give a straight line with an intercept of the initial pulse width squared, t_o^2. Figure 14 shows such a plot for a major negtive reactant ion peak with the voltage varied from -2000 to -4000 V in 100 V increments, at an entrance gate width of 0.20 ms.

The least-squares line fit to the data points in Figure 14 has an intercept of 0.06923 ms^2 for t_o^2, corresponding to a value of 0.263 ms for the initial pulse, width, t_o. This is compared to the actual pulse width applied to the gate of 0.200 ms. This extrapolated value may be associated with peak broadening by all processes except diffusion. The magnitude of these effects can be estimated by modifying Equation 24 to:

$$T_{1/2}^2 = t_o^2 + t_{1/2}^2 + t_x^2 \quad (27)$$

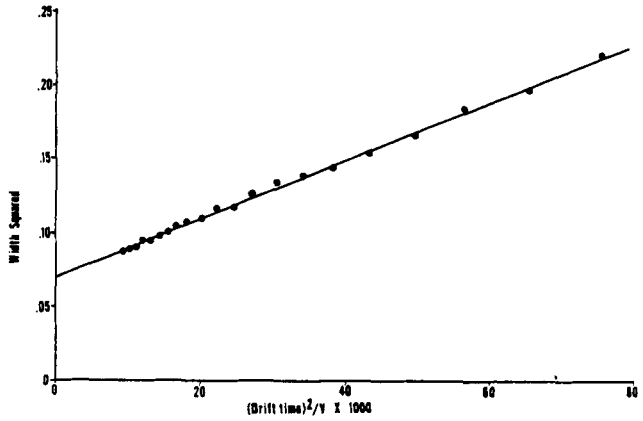

FIGURE 14. IMS peak width squared vs. drift time squared divided by the voltage. The value at the intercept allows calculation of peak broadening caused by factors other than initial pulse width or diffusion. Details in text, section entitled Resolution.

where t_x is the half width associated with broadening from effects other than diffusion and the initial pulse width. In the above case, $t_o^2 + t_x^2 = 0.0693$. Using 0.200 for t_o, band broadening due to other effects, t_x, can be estimated at 0.171 ms.

The experimental curves in Figures 11 and 12 can now be explained. The shape of the resolution vs. $E^{1/2}$ curves in Figure 12 is related to the relative contributions of the diffusional width, $t_{1/2}$, and the initial width, t_o, to the overall peak width, $T_{1/2}$. At low electric fields and with narrow gate pulses, the diffusional width is dominating and experimental resolution increases with voltage, as expected from Equation 23. As the electric field increases, however, the diffusional width decreases and the initial pulse width becomes dominant. Once the initial width becomes the major component of the total pulse width, increasing the voltage moves the drift time, t_d, closer to the origin without appreciably narrowing the total pulse width, $T_{1/2}$. Thus, resolution ($R = t_d/2T_{1/2}$ decreases with increasing electric field.

In Figure 11, the increasing resolution with drift time can be accounted for by the decreasing importance of t_o in the total pulse width at longer drift times. At approximately 16 ms, the curve is approaching the result expected from Equation 23 for diffusion-controlled resolution, i.e., resolution being independent of drift time.

V. ATMOSPHERIC PRESSURE IONIZATION — DYNAMICS

An excellent discussion of the chemical dynamics of atmospheric pressure ionization with a ^{63}Ni source has been previously published.[69] This article pointed out that atmospheric pressure ionization is determined by the interplay between five major chemical rates:

1. Primary ionization, providing reactant ions and/or thermal electrons
2. Ion-molecule reactions between reactant ions/thermal electrons and analyte molecules yielding product ions
3. Recombination reactions between positive and negative ions
4. Diffusion of positive and negative ions to the walls of the ionization source
5. Ventilation, which can be separated into three components: first, the flow of neutral gases and analyte molecules into the source, second, the flow of reactant and product ions out of the source, finally, the flow of neutral gases, unionized neutral analyte molecules, and neutral recombination products out of the source

A. Reactant Ion Formation

In one step or several very rapid steps, primary ionization from β-rays produces from the carrier gas both positive and negative reactant ion species, R^+ and R^-. R may denote different molecular structures and very often R^- will represent thermal electron, e^-. The rate of reactant ion formation per unit volume is estimated from the activity of the β-ray source using the approximation that one positive-negative ion pair is produced for each 35 eV of primary energy.[70] A radioactive source of C_A mCi, and W eV mean β-ray energy thus produces $C_A \times (3.7 \times 10^7)$ disintegrations per second $\times$ W_A eV per disintegration $\times$ one ion pair per 35 eV $\approx$ one $\times$ 10^6 $C_A W$ reactant ion pairs per second.

$$S = 1 \times 10^6 C_A W/V_S \tag{28}$$

S is the reactant ion pairs formed per second per unit volume, V_S is equal to the ion source volume, C_A is the source activity in mCi, and W is the mean β-ray energy in eV per disintegration. Under conditions where no sample is present, reactant ions are lost by recombination, diffusion to the walls, and flow out of the source. The steady-state reactant ion concentration for positive ions, R^+, can be expressed:

$$d[R^+]/dt = O = S - K_{Ri}[R^+][R^-] - \frac{D}{\langle X^2\rangle}[R^+] - \frac{F_C}{V_S}[R^+] \tag{29}$$

S is the reactant ion production rate. $K_{Ri}[R^+][R^-]$ is a positive-negative recombination term. $D[R^+]/\langle X^2\rangle$ expresses the loss of reactant ions by diffusion to the walls, D being the ionic diffusion coefficient and $\langle X^2\rangle$ is the mean square distance from points in the ion source volume to the walls. $F_C[R^+]/V_S$ is the loss of reactant ion density due to flow out of the ion source, F_C being the volumetric carrier gas flow rate.

A similar equation holds for negative ions, R^-. Under typical β-ray source activities (1 to 20 mCi), reactant ion density is dominated by the production and recombination terms, with diffusion and ventilation essentially negligible.[69]

B. Product Ion Formation

Product ions are produced by ion-molecule reactions between reactant ions and analyte molecules. Product ions are lost by recombination, diffusion, and ventilation. The steady-state rate equation for positive analyte ions, A^+, can be expressed:

$$\frac{d[A^+]}{d_t} = 0 = K_+ [R^+][A] - K_{R2}[R^-][A^+] - K_{R3}[A^-][A^+] - \frac{D_a[A^+]}{\langle X^2\rangle} - \frac{F_C[A^+]}{V_S} \tag{30}$$

Successive terms represent product ion formation, recombination between positive product ions and negative reactant ions, recombination between positive and negative product ions, diffusion of positive product ions to the walls, and the flow of positive product ions out of the source. Simplifying (detailed in Reference 69) yields an equation for the sample ion concentration per sample molecule concentration.

$$\frac{[A^+]}{[A]} = \frac{K_+ [R_o^+]}{K_+ [A] + K_R [R_o^+] + \frac{D_a}{\langle X^2\rangle} + \frac{F_C}{V_S}} \tag{31}$$

where $[R_o^+]$ = the reactant ion concentration with no analyte molecules present and K_R is a generic recombination rate. From Equation 31, estimates of the minimum and maximum detectable quantities can be made. Substituting typical values will show that

$$[K_R][R_o^+] >> \frac{D_a}{\langle X^2\rangle} + \frac{F_C}{V_S} \tag{32}$$

Therefore, the trace sample signal is controlled by the ratio of the product ion formation constant, K^+ to the recombination rate constant, K_R.

$$[A] \xrightarrow{\lim} 0 \frac{[A^+]}{[A]} = \frac{K_+[R_o^+]}{K_+ [A] + K_R [R_o^+]} = \frac{K_+}{K_R} \tag{33}$$

The maximum measurable signal is limited by the reactant ion concentration.

$$A \xrightarrow{\lim} \infty \frac{[A^+]}{[A]} = \frac{K_+ [R_o^+]}{K_+ [A] + K_R [R_o^+]} \tag{34}$$

$$\lim [A^+] = \frac{K_+ [R_o^+] A}{K_+ A} = [R_o^+] \qquad (35)$$

VI. IONIZATION SOURCES

A. Radioactive Ionization

The most common source in IMS, and the one used in the original plasma chromatographs[1,2] is a radioactive ^{63}Ni foil, analogous to those used in electron capture detectors. Other radioactive sources which have been or could be employed are listed in Table 1, along with several important parameters. These parameters include the type of particle emitted, the energy of the particle, the energy of gamma (γ) emission, and the half-life. The ideal source would be of low particle energy, producing a small number of ion pairs per disintegration thus minimizing fluctuations in ion current and hence noise level. An α-emitter, producing approximately 10^5 ion pairs per centimeter of travel, could be expected to generate high detector noise.[71] γ-emitters present a significant radioactive hazard. Low energy β-emitters thus appear most suitable. Commercially, tritium and ^{63}Ni are most important. Tritium has the advantages of lower energy, and higher specific activity foils are readily prepared. ^{63}Ni is most commonly used, due to its high temperature operation stability (400°C) compared to Ti^3H_2 (225°C) and Sc^3H_3 (325°C). The discussion that follows refers to ^{63}Ni radioactive ionization.

Table 1
General Characteristics of Possible Radiation Sources

Source	Particle	Energy (MeV)	γ (MeV)	Half-life (years)
^3H	β	0.018	0	12.5
^{99}Tc	β	0.292	0	$5 \cdot 10^5$
^{226}Ra	α	4.795	0.64	1622
		4.611	0.420	
		4.21	0.260	
			0.188	
^{241}Am	α	5.476	0.06	457
		5.433	0.04	
			0.10	
^{90}Sr	β	0.55	0	28
^{63}Ni	β	0.067	0	85
^{85}Kr	β	0.67	0.25	10.8
^{147}Pm	β	0.23	0.121	2.6

^{63}Ni emits β particles of energies forming a continuous distribution from 0 to 6.7×10^4 eV.[72] The β particles lose energy during collisions with the drift gas; the average energy loss per ion pair formed in N_2 is 35 eV, with ionization occurring as long as the energy of the β particles remains above the ionization potential of N_2, 15.58 eV.[73] The process is summarized in the following equation:

$$N_2 + \beta \rightarrow N_2^+ + \beta' + e^- \qquad (36)$$

β' is a β particle of reduced energy following the reaction, and e^- is the electron produced upon ionization of the N_2. The N_2^+ initiates a series of reactions, subsequently leading to the formation of three positive reactant ion species, $(H_2O)_xH^+$, $(H_2O)_yNO^+$, and $(H_2O)_zNH_4^+$. Under typical N_2 drift gas flow rates, 600 to 1400 ml/min, the $(H_2O)_xH^+$ predominates. Reactant ion distributions have been found to vary with the drift gas flow rate.[74]

The formation of $(H_2O)_xH^+$ was studied using a pulsed electron-beam mass spectrometer,[75] at source pressures of 0.5 to 3.5 torr, with trace water concentrations of 0.3 to 10 mtorr. The postulated mechanism at 300 to 420K follows:

$$N_2^+ + 2N_2 \rightarrow N_4^+ + N_2 \qquad (37)$$

$$N_4^+ + H_2O \rightarrow 2N_2 + H_2O^+ \qquad (38)$$

$$H_2O^+ + H_2O \rightarrow H_3O^+ + OH \qquad (39)$$

$$H_3O^+ + H_2O + N_2 \rightarrow (H_2O)_2H^+ + N_2 \qquad (40)$$

$$(H_2O)_2H^+ + H_2O + N_2 \rightarrow (H_2O)_3H^+ + N_2 \qquad (41)$$

Etc.

The number of clustered waters, x, in $(H_2O)_xH^+$ is a function of the temperature and the partial pressure of water in the gas. At the conditions of the above experiment, x = 2, 3, or 4 predominated. At 298 degrees Kelvin, 700 torr, and 5 torr partial water pressure (21%, relative humidity), the clusters contained 5 to 8 water molecules.[76] At 433 degrees Kelvin, ambient pressure, and 5×10^{-3} torr partial water pressure (7 ppm), the $(H_2O)_xH^+$ ion peak contained x = 2 or 3 water molecules in a ratio of approximately 7:3.[77]

The mechanism for the formation of the $(H_2O)_yNO^+$ reactant ion has been hypothesized based on processes known to occur in the atmosphere.[7] N_2^+ and ·OH, are produced according to reactions 34 to 37, the OH radical then initiates the following reactions leading to the hydrated nitric oxide ions:

$$N_2^+ + OH \rightarrow OH^+ + N_2 \qquad (42)$$

$$OH^+ + H_2O \rightarrow H_3O^+ + O \qquad (43)$$

$$N_2^+ + O \rightarrow NO^+ + N \qquad (44)$$

$$NO^+ + H_2O + N_2 \rightarrow (H_2O)NO^+ + N_2 \qquad (45)$$

y = 0 or 1 were the predominant species observed in IMS-MS studies.[77]

The final reactant ion, $(H_2O)_zNH_4^+$, z = 0 or 1,[77] is probably obtained via proton transfer from the $(H_2O)_xH^+$ reactant ion to NH_3 contaminants from the atmosphere or NH_3 outgassing from the stainless steel drift rings.

$$NH_3 + (H_2O)_xH^+ \rightarrow NH_4^+ + xH_2O \quad (46)$$

$$NH_4^+ + H_2O + N_2 \rightarrow (H_2O)NH_4^+ + N_2 \quad (47)$$

1. Reactant Ions, Negative

With nitrogen used as both drift and carrier gas, the negative reactant species is the thermal electron. Using nitrogen as the drift gas, but air as the carrier gas, the principal charge-carrying species has been identified by IMS-MS studies as CNO^- and $O(H_2O)_2^-$.[78] With air used as both carrier and drift gas, O_2^- predominated.[78] Studies done by atmospheric pressure ionization-mass spectrometry identified primarily O_4^- when using dry air as carrier gas, but $(H_2O)O_2^-$ with wet air carrier gas.[79] Several trace reactant ions have also been identified including $(H_2O)OH^-$, Cl^-, NO_2^-, CO_4^-, and CN^-.[78]

2. Product Ions, Positive

Four basic ion-molecule reactions have been identified in the positive mode of IMS leading to the formation of positive product ions.

First, proton transfer reactions can occur if the proton affinity of the sample molecule is greater than that of the reactant ions.

$$(H_2O)_xH^+ + A \rightarrow AH^+ + xH_2O \quad (48)$$

Tables of gas phase proton affinities are available for numerous organic species.[80] A protonated water reactant ion will transfer its proton to most organic functionalities including alkenes, alcohols, ethers, aldehydes, ketones, carboxylic acids, esters, thiols, sulfides, nitriles, and amines. This reaction is rapid and highly efficient. Ionization efficiencies measured in the authors' laboratory for tributylamine, a species of high proton affinity, are approximately 0.003 (or 0.3%).[46]

By doping the system with NH_3 vapors, a single reactant ion of the type $(H_2O)_zNH_4^+$ has been formed.[19] This reactant ion selectively ionizes those functionalities having greater proton affinity than ammonia.

$$(H_2O)_zNH_4^+ + A \rightarrow AH^+ + NH_3 + 2H_2O \quad (49)$$

In general, this includes only the nitrogen-containing compounds, amines, diamines, pyridines, and anilines.

Second, charge transfer reactions have been observed between the $(H_2O)_yNO^+$ reactant ion and benzene derivatives.[81]

$$\text{a)} \quad (H_2O)_yNO^+ + A \rightarrow A^+ + NO + yH_2O$$

$$\text{Ex)} \quad (H_2O)_yNO^+ + C_6H_6 \rightarrow (C_6H_6)^+ + NO + yH_2O \quad (50)$$

Third, electrophilic addition of NO^+ to nitroaromatics has been observed.[82,83]

$$\text{a)} \quad (H_2O)yNO^+ + A \rightarrow ANO^+ + yH_2O$$

$$\text{Ex)} \quad (H_2O)yNO^+ + O_2N\text{–}C_6H_4\text{–}OH \rightarrow [O_2N\text{–}C_6H_4\text{–}OH]\ NO^+ + yH_2O \quad (51)$$

Finally, hydride transfer from alkanes to the nitric oxide reactant ion has also been observed.[83]

$$(H_2O)_yNO^+ + C_nH_{2n+2} \rightarrow (C_nH_{2n+1})^+ + HNO + yH_2O$$

3. Product Ions, Negative

The major negative reactive ions $(H_2O)_nO_2^-$, and thermal electrons selectively ionize molecular species of high electron affinity by one of three general pathways.

1. Associative electron capture.[5]

$$AB + e^- \rightarrow AB^-$$

$$\text{Ex)} \quad O_2N\text{–}C_6H_5 + e^- \rightarrow (O_2N\text{–}C_6H_5)^- \quad (52)$$

2. Dissociative electron capture.[5,38]

$$AB + e^- \rightarrow A + B^-$$

$$\text{Ex)} \quad C_6H_5Cl + e^- \rightarrow C_6H_5 + Cl^- \quad (53)$$

3. Proton abstraction.[82]

$$ABH + e^- \rightarrow AB^- + H^+e^-$$

$$\text{Ex)} \quad O_2NC_6H_4OH + e^- \rightarrow (O_2NC_6H_4O)^- + H^+e^- \quad (54)$$

Iodobenzene and bromobenzene also have been found to form halide product ions through a dissociative electron capture mechanism. Aromatics with two different halogen substituents dissociate only the most reactive halogen ion in the order I > Br > Cl.[38] Chloronitrobenzene and decachlorobiphenyl undergo both associative and dissociative electron capture.[38] Mildly acidic species, such as substituted phenols, have been observed to form product ions by a proton abstraction mechanism. A

complex fragmentation/addition mechanism is suggested by the $[OC_6H_4NO_2]^-$ product ion found for para-chloronitrobenzene.[84] Several comprehensive works have been published on the electron capture process.[71,73,85]

Acetone[20,86] and chloride[21,42] reactant ions have been used to improve selectivity and specificity of ionization providing simpler and more sensitive ion mobility spectra. The most common negative reactant ion in purified air has been shown to be O_2^- clustered with H_2O. For chloride ion chemistry, the electron affinity of chlorine (3.58 to 3.70 eV) is greater than that for O_2 (0.15 to 1.20 eV).[87] This allows the charge to transfer from the oxygen ion to the chlorine neutral molecule. It has been postulated that for the chloride ion to lose its charge to a sample molecule the molecule must have a larger electron affinity.[42] Since only a limited number of compounds exceed chlorine on the electron affinity scale, selectivity in IMS can be achieved by using chloride ion/molecule reaction chemistry.

Nitrocompounds, such as explosives, can be observed in the presence of chloride ion due to their high electron affinity. For example, Figure 15 demonstrates spectra of ethylene glycol dinitrate (EGDN), a common impurity in dynamite. The lower spectra was obtained in zero grade nitrogen and exhibits five mass identified peaks, indicative of complex ionization chemistry involving dissociation, electron capture, and dissociation adduct chemistry. The upper spectra obtained in the presence of Cl^- reactant ions displays much greater specificity of ionization, with a large peak due to associative adduct reaction predominating.

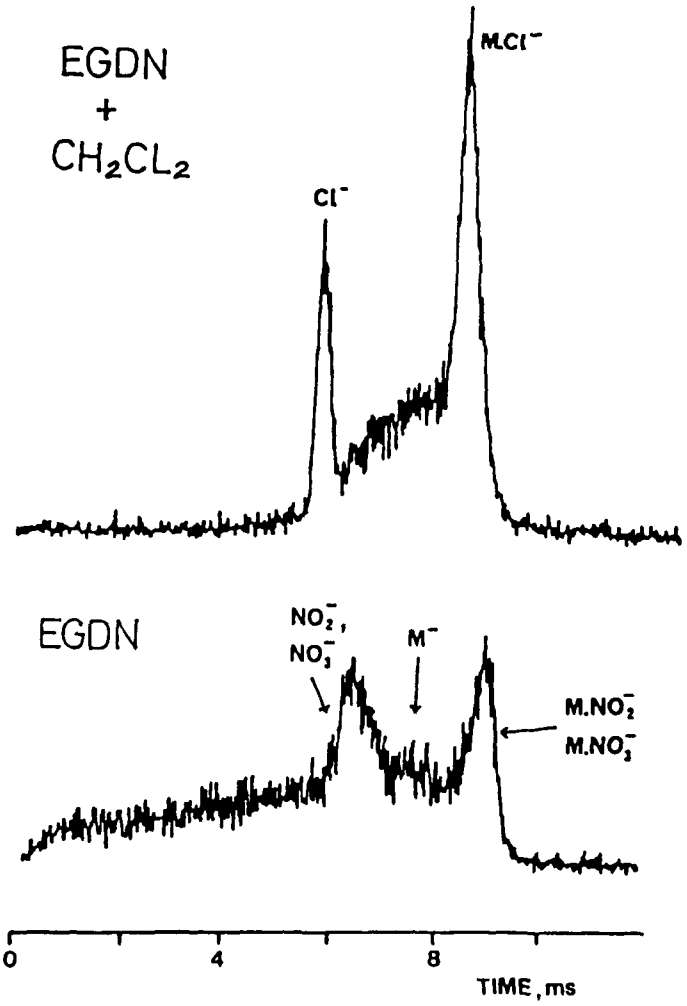

FIGURE 15. Lower tracing is negative ion mobility spectra of EGDN in nitrogen. Upper spectra was obtained using chloride reactant ions. (Reprinted from Proctor, C. J. and Todd, J. F. J., *Anal. Chem.*, 56, 1794, 1984. With permission.)

B. Photoionization

When a compound is irradiated with UV light, ionization occurs if the ionization potential of the compound is less than or equal to the photon energy.

$$R + h\upsilon \rightarrow R^+ + e^- \qquad (55)$$

This type of ionization process has two fundamental advantages over ^{63}Ni ionization. First, it is a primary ionization process and consequently its linear range is not limited by reactant ion concentration. Linearity over five orders of magnitude has been demonstrated.[63] Second, ion mobility spectra created via photoionization contain no reactant ions. Consequently, the entire mobility spectrum from 0 to 25 ms can be used for monitoring product ions. Thus, the region of a mobility spectrum normally occupied by reactant ions in a ^{63}Ni source is free of background ions with PI-IMS and can be used for detection of ions which drift in this region.

Response characteristics of the photoionization detector, PID, used in gas chromatography for selective detection of aromatics and other unsaturated organics have been reviewed by several workers.[88-91] PID design consists of a UV lamp separated from the ionization region by a transparent UV window, typically composed of MgF_2 or LiF. The analyte is swept into the ionization cell by an inert carrier gas and exposed to the monochromatic UV photons (common lamp energies are 9.5, 10.2, and 11.7 eV). When the analyte's ionization potential is less than the energy of the photons, ionization occurs. Positive ions formed are collected at the cathode and photoejected electrons are collected at the anode to create the analytical signal. The same general process occurs in photoionization-IMS, except the positive ions are directed into the IMS to be separated and detected via their mobility characteristics.

The processes involved in photoionization are summarized below:

$$AB + h\upsilon \rightarrow AB^* \quad R_1 = I^\circ - I \qquad (56)$$

$$AB^* \rightarrow AB^+ + e^- \quad R_2 = K_2[AB^*] \qquad (57)$$

$$AB^* \rightarrow A + B \quad R_3 = K_3 [AB^*] \tag{58}$$

$$AB^* + C \rightarrow AB + C \quad R_4 = K_4[AB^*] [C] \tag{59}$$

$$AB^+ + e^- + C \rightarrow AB + C \quad R_5 = K_R[AB^+] [e^-] \tag{60}$$

$$AB^+ + \text{Cathode} \rightarrow i, \text{signal} \quad R_6 = K_6[AB^+] \tag{61}$$

AB is the analyte molecule, C is the carrier gas, R is the reaction rate, * indicates an excited state, I° is the initial photon flux, I is the transmitted radiation, I°-I thus being the number of photons absorbed per second.

The probability that a photon will be absorbed (Equation 57) depends on the absorption cross section, σ, of the molecule AB as defined by the Beer-Lambert Law.

$$I = I°\exp(-\sigma N_L V_N [AB] L) \tag{62}$$

N_L is the Loschmidt number (2.69×10^{19} molecules/cm^3), V_N is the volume of 1 mol of gas at stp, and L is the photo path length (cm). The transmitted radiation, I, decreases exponentially with increasing cross section and analyte concentration. Since absorbance is equal to $-\ln I/I°$, it will increase linearly with absorption cross section, σ, and concentration.

The probability of ionization after photon absorption depends on the photoionization efficiency, η.

$$\eta = \frac{K_2}{K_2 + K_3 + K_4} \tag{63}$$

This efficiency is the ratio of the excited analyte molecules that are ionized to the total number of excited molecules. Once excited by absorption of a photon, analyte molecules can proceed to ionize (Equation 58), they can dissociate into neutral fragments (Equation 59), or they can be quenched by collisional relaxation with the carrier or drift gases (Equation 60). If recombination of ionized molecules is minimized by using a high electric field,[90] the ionization current of the detector can be written:

$$i = I° \eta \sigma N_o FL [AB] \tag{64}$$

N_o is Avagadro's number, and F is Faraday's constant. [AB] is the gas phase concentration of the analyte molecule. While reported detection limits[63] using photoionization-IMS are some two orders of magnitude less sensitive than ^{63}Ni ionization, response is concentration dependent and sensitivity improvements are possible by further reduction of the cell volume. Detection limits of femtograms have been reported for a PID of <50 μl cell volume.[92]

Two basic photoionization cell designs have been reported for use with IMS, one with a 10.0-eV krypton lamp perpendicular to the drift gas flow, as illustrated in Figure 16. This

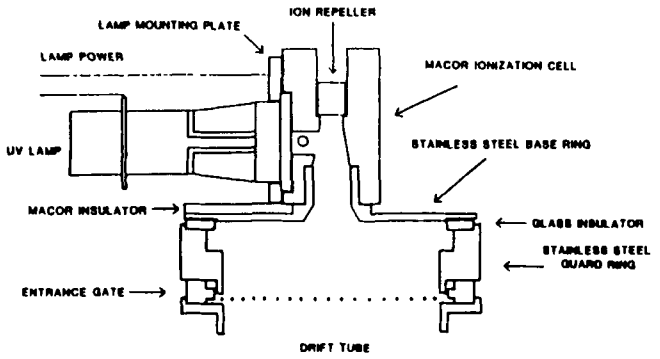

FIGURE 16. Schematic drawing of photoionization source. UV lamp is perpendicular to drift axis.

system provided reliable response using N_2 drift gas and has been used as a detector after capillary gas chromatography.[15,63] The second design[93] consisted of an on-axis 10.2-eV hydrogen discharge lamp, as illustrated in Figure 17. Ionization of analyte molecules beyond the entrance gate and photoejection of electrons from the collector probably limit the usefulness of the on-axis design. Detection limits of the on-axis design were reported to be 0.1 to 50 ppb with working ranges of 10^3 to 10^4.[93] Minimum detectable amounts using the perpendicularly positioned krypton lamp were approximately 1 ng, with response linearity of five orders of magnitude.[63]

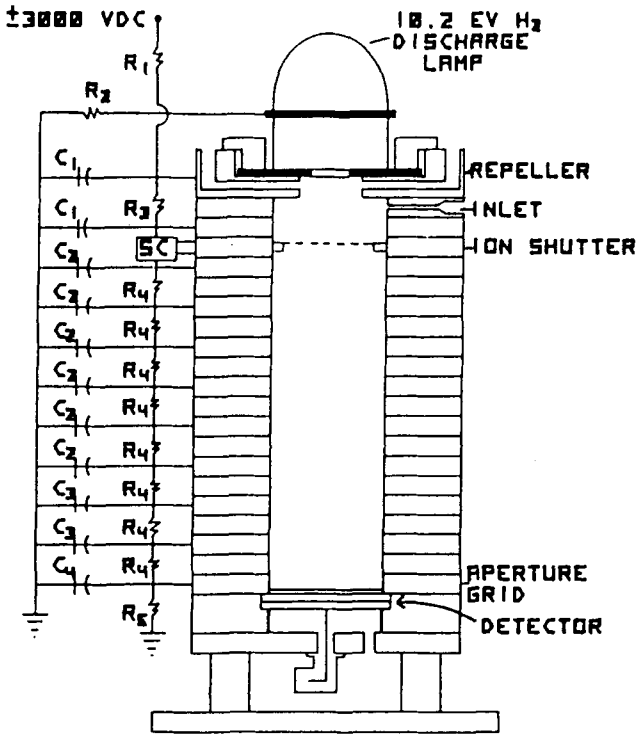

FIGURE 17. Schematic drawing of ion mobility spectrometer with on-axis hydrogen discharge lamp for photoionization. (Reprinted from Leasure, C. S., Fleischer, M. E., Anderson, G. K., and Eiceman, G. A., *Anal. Chem.*, 58, 2142, 1986. With permission.)

C. Laser Ionization

A laser ionization IMS is illustrated in Figure 18. Selective ionization for IMS is sometimes possible using a tunable Nd:YAG pumped pulsed laser system.[16,94] If a laser source is tuned to an excited electronic energy state of an analyte molecule, a multiphoton ionization process is greatly enhanced. Since the density of energy states above the excited intermediate state are usually quite high, subsequent absorptions are resonant or nearly resonant. Excitation from the intermediate state to the ionization continuum is quite rapid and may involve the absorption of up to six additional photons. The transition to the lowest intermediate state is generally the rate-limiting step. If the laser is not tuned to an intermediate state, the probability of ionization is slight. In resonant two-photon ionization (R2PI), the first photon excites the molecule into the intermediate state, while the second photon ionizes the molecule. Figure 19 illustrates a nonresonant multiphoton ionization process and a resonant enhanced two photon ionization process.

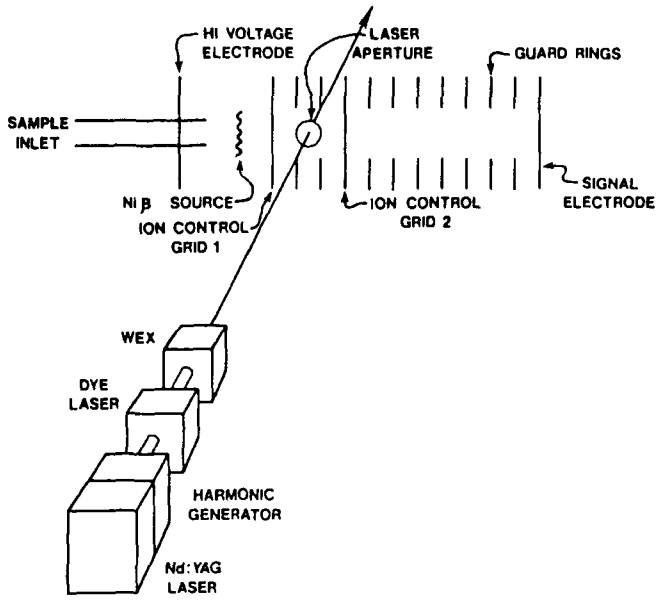

FIGURE 18. Plasma chromatograph modified for use with laser ionization. (Reprinted from Lubman, D. M. and Kronick, M. N., *Anal. Chem.*, 54, 1546, 1982. With permission.)

An ArF excimer laser operating at 194 nm has been introduced as a general ionization source, capable of ionizing the vast majority of organic compounds.[95] At the power levels required to ionize the organic molecules, stable atmospheric gases such as O_2, N_2, and CO_2 were not ionized.

Figure 20 demonstrates selectivity in IMS based upon the wavelength of the ionizing laser light.[95] Figure 20 shows the laser-induced mobility spectrum of p-xylene and n-methylaniline at a wavelength of 266 nm. Two overlapping peaks are

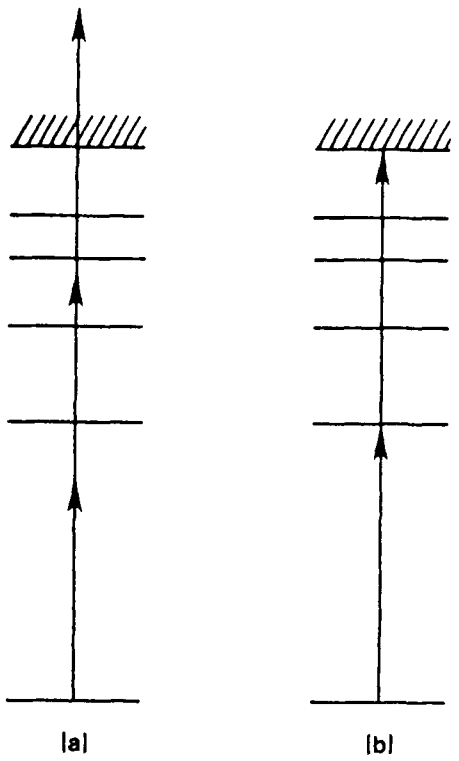

FIGURE 19. Multiphoton ionization processes: (a) nonresonant multiphoton ionization; probability of ionization is low. (b) Resonant enhanced two-photon ionization; much greater probability of ionization. (Reprinted from Lubman, D. M. and Kronick, M. N., *Anal. Chem.*, 54, 1546, 1982. With permission.)

evident. At a wavelength of 310 nm (Figure 20b), n-methylaniline has been selectively ionized. The same reference[95] demonstrates selective ionization of m-toluidine (K_o = 1.94) from 2,4-lutidine (K_o = 1.95), and diisopropylamine (K_o = 1.93) from hexylamine (K_o = 1.95) based upon the energy of ionization. The potential usefulness of the technique is certainly demonstrated.

A study[61] comparing the reduced mobilities of ions produced by resonance-enhanced two photon ionization to ^{63}Ni-produced ions found little variation (±2.5%). This was confirmed in an additional study[64] using N_2, air, argon, argon-methane, and CO_2 as drift gases. Laser-produced ions introduced into a quadrupole mass spectrometer revealed the molecular ion M^+ or MH^+ with no fragmentation, in almost every case, for aromatics, polyaromatics, and substituted aromatics.[64]

The effects of various laser beam parameters on IMS sensitivity and resolution have been studied.[96] Response varied directly with laser beam energy and inversely with laser beam size. Quantitative accuracy in laser-IMS with a pulse ND:YAG laser was limited by inhomogeneity of the beam cross section and variations in beam energy between pulses.[96] Increased spectral band broadening, relative to ^{63}Ni spectra, was also reported.[96]

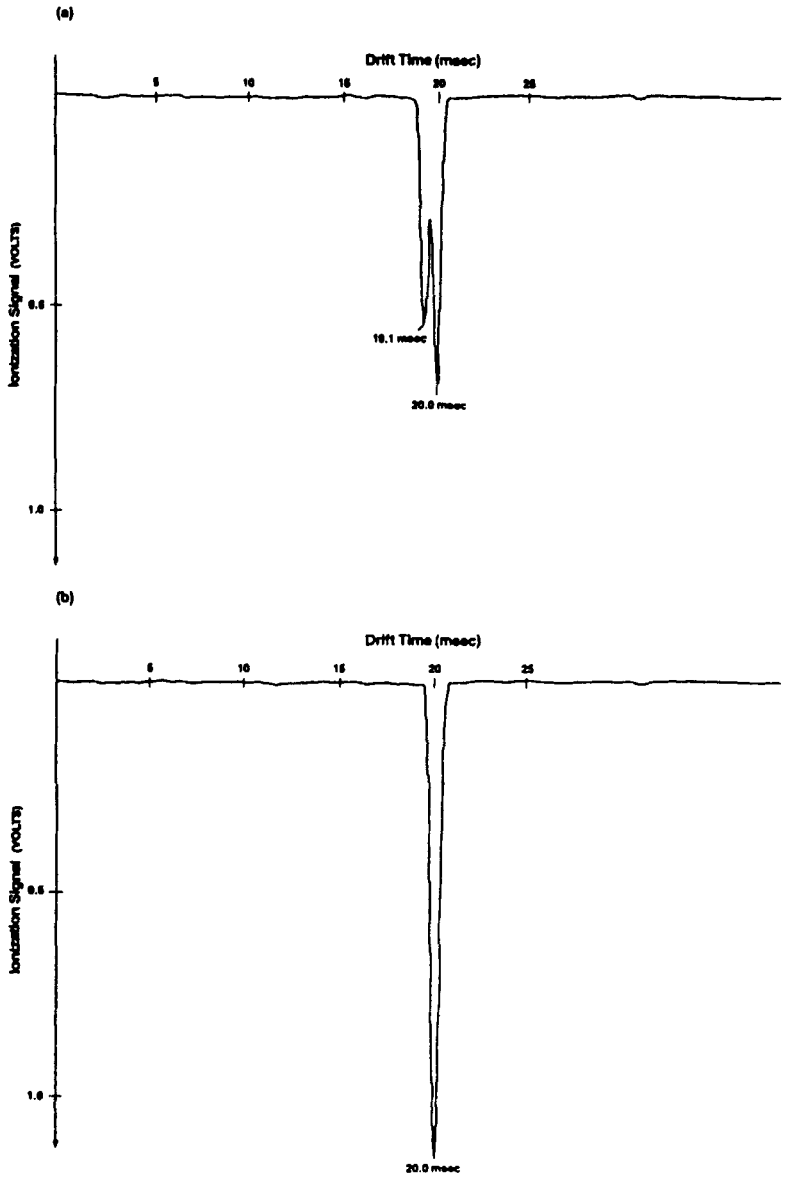

FIGURE 20. Laser-induced ion mobility spectrum. (a) Ionizing wavelength of 266 nm. Two peaks are product ions of p-xylene and n-methylaniline. (b) Ionizing wavelength of 310 nm. Selective ionization of n-methylaniline demonstrated. (Reprinted from Lubman, D. M. and Kronick, M. N., *Anal. Chem.*, 54, 1546, 1982. With permission.)

D. Surface Ionization

An ionization source has been designed[18] for the detection of N- and P-containing molecules, based upon the principles of the thermionic ionization detector.[97] The ion source includes an alkali-metal impregnating a thermally stable glass or ceramic bead. The bead is immersed in a gaseous mixture of H_2 and air and resistively heated to 200 to 1000°C. Selective ionization of P- and N-containing molecules is obtained upon contact with the bead.

A related source has also been described.[98] Selective ionization via electrolytic reactions is accomplished by introduction of inorganic/organic salts into the source. Reactions between the sample molecules and electrolytic salts create product ions. Salts may be alkali/halogen, alkali acid, ammonium, alkaline earth, transition metal, or complex organic salts. An electric field is applied to the surface of the electrolyte to assist the movement of ions from the surface into the gas.

E. Electrified Spray Ionization

The driving force to this research is the desire to develop a universal and sensitive detector for liquid samples. The applicability of electrified spray-IMS as a detection method for

high performance liquid chromatography (HPLC), ion chromatography, capillary zone electrophoresis, and field flow fractionation is currently under investigation.[99] A solution carrying the analyte of interest is sprayed from the tip of an electrically charged needle, producing charged droplets in an inert gas at atmospheric pressure.[100] As the solvent is evaporated from the drop, a residual molecular ion is formed. Recent studies[101] seem to indicate a secondary ionization process of the analyte molecule, the product ion being formed via a charge transfer process from a solvent/reactant ion. An excellent discussion of the behavior of evaporating electrically charged droplets has been published.[102] The electrofied spray phenomena can be subdivided into two regions, coronaspray and electrospray. The distinction is determined by whether the electric field on the ionizing needle is sufficient to produce a continuous corona discharge, in which case it is referred to as coronaspray. The process at lower fields is electrospray. While reduced noise characteristics are evidenced at lower fields, the electrospray region has exhibited less reliable ionization properties.[101] Mass spectroscopic studies of sprayed ions have demonstrated variations in the ions formed dependent upon temperature, field strength, and the gas in which the electrospray occurred.[103] Electrospray ion mobility spectra have been obtained for lysozyme in ethanol,[100] polystyrene, and polyvinylpyrolidine,[104] although resolution was poor.

Coronaspray-ion mobility spectra of several large polar molecules have been obtained using a unidirectional flow IMS.[101] Improved resolution was demonstrated, relative to the earlier electrosprayed spectra. Resolution comparable to that achieved by ^{63}Ni or photoionization methods has not yet been achieved. Initial results with coronaspray IMS as a detector for HPLC are presented in the chromatography section.

VII. SPECTRAL COLLECTION

Five general methods are available for the recording of ion mobility spectra. These include single scan, signal averaging, moving second gate, Fourier transform,[28] and a method based on nonlinear electric fields.[105]

A. Single Scan Method

The single scan method acquires an entire ion mobility spectrum from one entrance gate pulse. The exit gate is held open throughout the entire scan time or can be removed entirely from the drift tube. Total data collection time is rapid (25 to 50 ms), and this method can thus be used to monitor concentrations varying quickly with time. Unfortunately, the speed of collection requires a consequent sacrifice in sensitivity. This method, as well as the signal averaging method, requires extremely fast electrometers with rise times of less than 0.1 ms.

B. Signal Averaging Method

Signal averaging is similar in operation to the single scan method, except that a succession of scans are stored and then averaged to produce a single ion mobility spectrum. Signal averaging enhances the ion signal relative to the random noise. Very rapid data collection (1.6 s for 64 scans of 25 ms) was achievable with a detection limit of 200 ppt TNT.[46] The method is inherently limited, however, by the spectral resolution/sensitivity trade off connected with the duration of the entrance gate pulse, t_o. The resolving power of the system can never be less than the entrance gate pulse, thus a desire for short entrance gate durations. The maximum sensitivity, however, is a function of the entrance gate pulse divided by the total scan time, t_o/T_s. As resolution is enhanced by reducing t_o, the sensitivity is sacrificed. For example, with an entrance gate pulse of 0.25 ms, and a total collection time of 25 ms, the maximum current possible is

$$\begin{aligned} i &= (t_o/T_s)\, i_o \\ i &= (0.25/25)\, (i_o) \\ i &= 1/100\, i_o \end{aligned} \qquad (65)$$

The current sampled is only 1/100 of the total available current, i_o. The value of t_o/T_s is known as the spectral sampling fraction.

C. Fourier Transform Method

In order to make better use of the available ion current, the Fourier transform method of spectral collection was devised.[28] Fourier transform spectral collection is unique in several ways: (1) the gate signals are controlled by a binary (on, off) scanning square wave generator; (2) the entrance and exit gates are driven simultaneously by the same square wave with zero phase delay; (3) the scanning parameter is the square wave frequency; (4) Fourier transformation of the frequency dispersive interferogram produces the familiar time dispersive ion mobility spectra.

With this method, both the entrance and exit gates are open 50% of the time. Half of the ions pass the entrance gate, 50% of those pass the exit gate, so 25% of the total available ions are sampled. Since the signal/noise enhancement increases with the square root of the ratio of the sampling fractions, the possible enhancement is $\sqrt{25\%/1\%} = 5$ over the signal/noise obtained for the previously mentioned signal averaging parameters. Experimental comparisons of Fourier transformation to signal averaging spectral collection under conditions of equal instrumental resolution and data collection times show enhancement factors of 1.4 to 2.4 for the FT method.[46] The maximum theoretical enhancement was not obtained due to increased noise levels in the interferogram, portions of which appear to be signal related. Small improvements in resolution were also measured with the FT methodology.

A related method uses a software second gate. In this method, all the ions admitted through the entrance gate reach the collector producing a sampling fraction of 50%, and a possible enhancement factor over the signal average method of $\sqrt{50\%/1\%} = 7$. In this method, the data are exit gated with a software multiplication factor, forming two interferograms

180° out of phase. After transformation, the two spectra are averaged to produce the enhanced signal. The theoretical enhancement has not yet been achieved. FT spectra with data collection times of 0.25 s have been obtained.[46]

D. Scanning Second Gate Method

The scanning second gate method[106] is electronically simple but extremely slow. To obtain the ion mobility spectrum, the entrance gate is pulsed open for a preselected length of time at a fixed frequency. For example, it can be pulsed open for 0.25 ms every 25 ms. The time delay between the closing of the entrance gate and the opening of the exit gate is slowly increased from 0 to 25 ms. In this manner, ions with increasingly longer drift times are allowed to reach the collector. A complete ion mobility spectrum typically takes a few minutes to produce, limiting the usefulness of the technique to those situations where the qualitative and quantitative concentration is invariant over several minutes.

E. Other Methods

A recent article[105] presented ideas for enhancing sensitivity and selectivity using nonlinear electric fields, and bidirectional fields (a forward field moving ions toward the collector, a reverse field moving ions back toward the entrance gate). Although these ideas are interesting, no experimental data, instrumental details, or collection times were presented.

VIII. IMS AS AN ANALYTICAL SPECTROMETER

IMS has several strengths that enhance its suitability as a technique for trace air quality monitoring.[25] First, it is an extremely sensitive technique with sub-parts-per-billion or picogram detection limits for many compounds. Second, it has a selectivity factor based on ion mobility and/or field polarity that allows specificity of detection in the presence of matrix interferents. Third, IMS has continuous real-time monitoring capabilities with virtually no time delay between sampling and measurement. Fourth, the system can be easily automated to perform suitable sampling, calibration, and data analysis of one or more compounds at below parts-per-billion concentration levels for extended time periods.

Unfortunately, IMS also has some serious weaknesses that limits its applicability to trace air quality monitoring. First, IMS has a limited linear range. A response vs. concentration plot (Figure 21) for hexafluoroacetone is substantially linear from the lower detection limit of 3 to 50 ppb, after which the response begins to level off; above 100 ppb the response is essentially constant. This response pattern is due to the limited number of reactant ions available for ion molecule reactions with analyte molecules.

A second major weakness of IMS is the response variation that occurs with different background gas composition. Figure 22 shows the changing peak intensity for 10 ppb of *N*-nitrosodimethylamine (NDMA) as varying types and concentrations of contaminants were introduced into the detector. Peak intensity of the ion of interest depends on complex ion-molecule equilibria among all species. The net extent of ionization depends on the reaction kinetics of the analyte, as well as reaction properties of the contamination. Consequently, in a changing

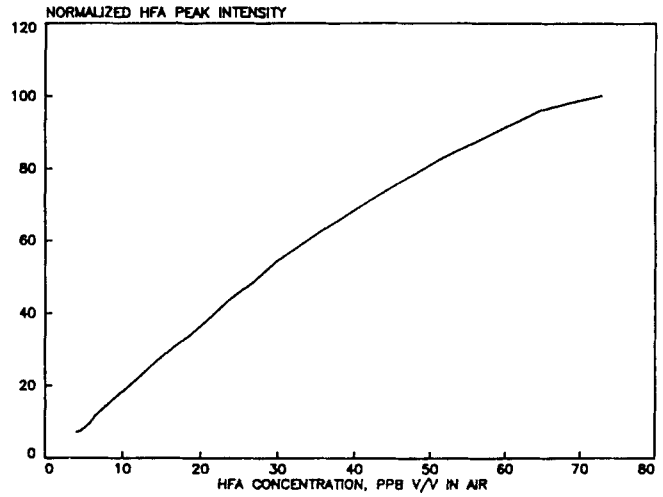

FIGURE 21. Peak intensity vs. molecular concentration of hexafluoroacetone (HFA) in laboratory air. Product ion measured was identified as HFA (O_2) — by IMS/MS. (From Dam, R. J., in *Plasma Chromatography*, Carr, T. W., Ed., Plenum Press, New York, 1984. With permission.)

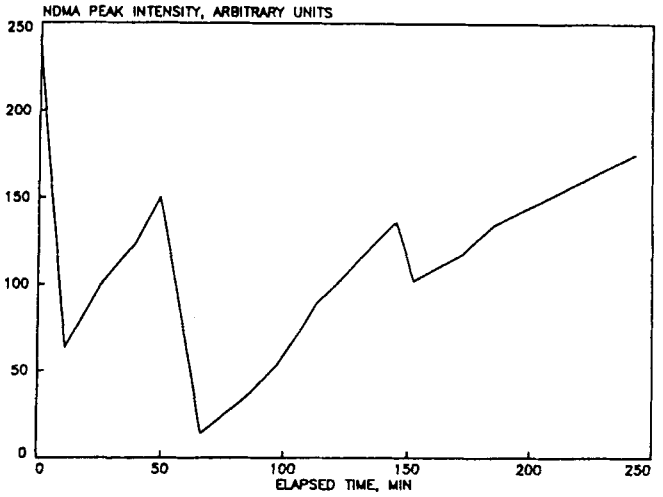

FIGURE 22. Peak intensity of 10 ppb of *N*-nitrosodimethylamine (NDMA) in the presence of varying contaminants. Experiment began with clean laboratory air; added were dimethylamine, 10 ppm, at t = 0 min; ethylbenzoate, 1 ppm, at t = 39 min; bis-2-methoxyethyl ether, 50 ppm, and ethylenediamine, 25 ppm, at t = 50 min; and 1,2-dimethyoxyethane, 50 ppm, at t = 140 min. NDMA peak intensity changed significantly with the addition of contaminants even though its concentration was constant. (From Dam, R. J., in *Plasma Chromatography*, Carr, T. W., Ed., Plenum Press, New York, 1984. With permission.)

background matrix, peak intensity alone is insufficient to provide quantitative analysis. This problem can be circumvented using a prior clean up/separation step such as gas chromatography, but real-time monitoring is then sacrificed. DuPont Corporation has devised a calibration technique that minimizes the effects of background variation.[25] Its basic concepts follow; derivation of the method is provided in the original reference.

This calibration technique takes into account the possibility that every sample contains a unique background composition against which the concentration of one or several molecules of interest is to be measured. Each IMS measurement is accompanied by a calibration. The calibration technique consists of known additions being made directly to the sample stream and the combined analyte/addition response is used to calculate the analyte concentration. It is referred to as the trace addition method and resembles the well-known standard addition method, but several features unique to IMS are used in its derivation. A major advantage of this method is that it does not require specific knowledge of the background composition and reaction kinetics.

Let A be the molecule of interest, and B, C, ... be other molecules in the background gas. C(A), C(B), C(C) are the concentrations of A, B, and C, respectively. I(A) is the measured ion intensity of the peak corresponding to A. Consider a hypothetical response function for A:

$$I(A) = C(A) \cdot F[C(A), C(B), C(C), \ldots] \quad (66)$$

The value of the response, I(A), is a function of the concentration of A multiplied by another function, F, of the concentration of all the molecules present (including A). The function, F, may be a very complex function and is implicitly a function of time since all the molecular concentrations are assumed to vary with time. It includes all ion-molecule interactions that affect the response. The equation derived for calculation of the concentration of analyte molecule A, C(A), was

$$C(A) \approx \left[\frac{\Delta(\ln I(A))_{ADD:A}}{\Delta C(A)} - K_7 \frac{\Delta(\ln I(A))_{ADD:B}}{\Delta C(B)}\right]^{-1} \quad (67)$$

$\Delta(\ln I(A))_{ADD:A}$ is the natural logarithm of the change in intensity of the response for A upon addition of a small standard concentration of A, $\Delta C(A)$. Likewise $\Delta(\ln I(A))_{ADD:B}$ is the natural logarithm of the change in intensity of the response for A upon addition of a small standard concentration of B, $\Delta C(B)$. The molecule B should have a response mechanism similar to A, in which case a change in background gas composition will affect both ion-molecule reactions similarly. In other words, if a change in the background matrix occurs, A and B will be affected in a like manner, both increasing or both decreasing, although potentially at a different rate, K_7.

This two-step standard addition accounts for both terms in Equation 66. $\Delta C(A)$ allows one to calculate $\Delta I(A)$ as C(A) changes and $\Delta C(B)$ allows one to estimate the change in F[C(A), C(B), C(C),...] as C(A) changes since B and A have similar ion-molecule reaction properties. This is generally true with structurally similar compounds of the same organic functionality.

Within the linear range of sample A, the F[C(A), C(B), C(C),...] term is essentially constant with changes in C(A), so Equation 67 reduces to the more familiar one-step standard addition:

$$C(A) \approx \left[\frac{\Delta \ln(I(A))_{ADD:A}}{\Delta C(A)}\right]^{-1} \quad (68)$$

or

$$C(A) \approx \frac{I(A)}{\Delta I(A)} \times \Delta C(A) \quad (69)$$

When the response is linear, the relative change in peak intensity is equal to the relative change in concentration. Use of the one-step addition can provide quantitative information only in the linear range, but can still provide alarm capabilities beyond this point. $\Delta I(A)/\Delta C(A)$ is a constant within the linear range. If $\Delta I(A)/\Delta C(A)$ is less than normally obtained in the linear range, an alarm can be sounded indicating that either the C(A) has risen above the linear level or that reactant ions have been depleted to a level providing unreliable information. The effectiveness of the one-step technique is demonstrated in Figure 23, showing the corrected response of 10 ppb NDMA in varying background matrices.

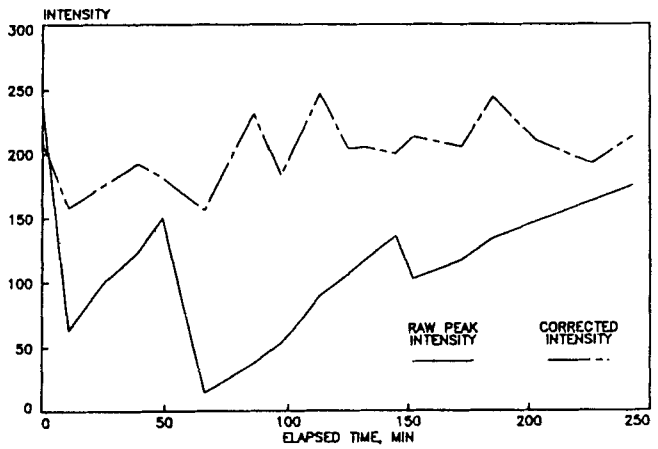

FIGURE 23. Application of the single-step calibration technique to the NDMA experiment of Figure 22. Whereas the raw signal intensity varied by a factor of 15, the corrected intensity varied by only 12% and exhibited less correlation with addition of background contaminants. (From Dam, R. J., in *Plasma Chromatography*, Carr, T. W., Ed., Plenum Press, New York, 1984. With permission.)

An additional advantage of the trace-addition calibration method is that it eliminates the need for relying on a single drift time or mobility value to identify a given ion in the drift spectrum. The precise drift time of the ion of interest can be determined from a difference spectrum of the sample plus addition and the sample. The analytical peak is typically the maximum in such a difference spectrum (Figure 24). Small variations in temperature, pressure, or other variables that affect ion drift times do not affect the identification of peaks used for analysis.

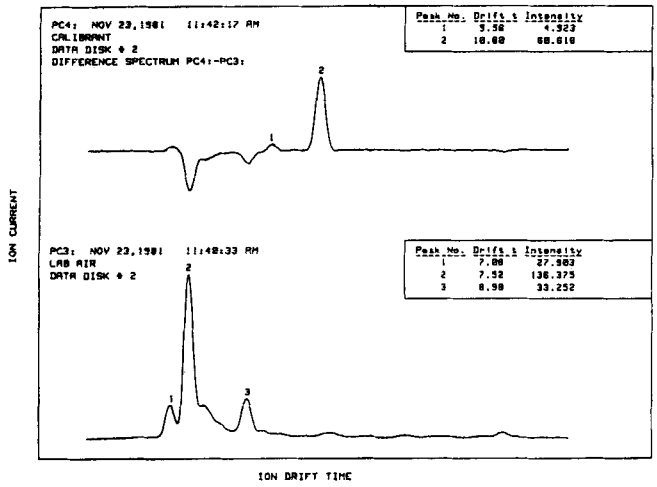

FIGURE 24. Spectrum PC3 is air in the negative-ion mode. To this sample was added a calibrant of 20 ppb perfluoropropionyl chloride, and a second spectrum was taken. The difference between the two spectra is shown at the top of the figure. Peak 2 of the difference spectrum is the peak used for analysis. (From Dam, R. J., in *Plasma Chromatography*, Carr, T. W., Ed., Plenum Press, New York, 1984. With permission.)

DuPont Corporation has used the technique to monitor airborne chemicals in work place environments. Table 2 shows a partial list of chemicals monitored. As with all analytical techniques, the suitability of IMS for a particular monitoring application must be approached on a case-by-case basis. Questions to be addressed include (1) limits of detection of the molecule in clean air; (2) identity and mobility of analyte product ions; (3) identities, concentrations, and mobilities of major background contaminants; (4) effect of contaminants on the sensitivity to the molecule of interest.

Several real-time monitoring applications are discussed in the literature. There is considerable current interest in detection of explosives,[42,107-109] chemical warfare agents, and drugs of abuse.[36,110,111] IMS systems are under consideration as screening devices for these substances on people and in materials. Additional applications include measurement of nickel carbonyl in air,[112,113] sensing of petrochemical fuels in the headspace of soils,[114] and the analysis of water, polymer outgassing, and surface contaminants in semiconductor devices and microelectronic packages.[84,115,116] An example application of IMS

Table 2
Plasma Chromatograph Toxic Monitoring Applications

Chemical	Detectivity[a]
Hexafluoroacetone	100 ppb
Dimethylcarbamyl chloride	0.5 ppb
Dimethyl sulfate	100 ppb
N-Nitroso dialkyl amines, C1-C4	0.5 ppb
Dimethylformamide	1.0 ppm
4-Aminodiphenyl	0.5 ppb
Hydrogen sulfide	30 ppb
Tetraethyl lead	0.01 mg/M^3

[a] Approximate lower detection limit on a V/V basis in clean laboratory air, except for tetraethyl lead which is on a weight basis as inorganic lead; detection limits will vary with different background conditions.

used as a preliminary screening device or as a tentative identifier is the use of skin surface sampling and IMS as a method for detecting drug residues on emergency room patients suspected of drug overdose.[36] The reduced mobility value provides tentative identification of a specific drug. Figure 25 shows representative spectra from a semiconscious patient who had taken an overdose of doxepin, a tricyclic antidepressant. A serum drug screen was positive for tricyclics. Advantages of the technique lie in its speed, sensitivity, and noninvasive method of sample procurement. Out of 101 instances of drug-related ingestion, 38 positive drug identifications were made.[36] This application demonstrates that for well-defined conditions IMS can be suitable for separation and tentative identification. However, for many trace analytical problems, matrices are complex, and high resolution preseparation processes, such as chromatography, are required.

IX. IMS AS A CHROMATOGRAPHIC DETECTOR

Many difficulties associated with IMS as an analytical technique are alleviated when using high-resolution chromatography as the method of sample introduction. Difficulties associated with unstable spectra under conditions of sample overload[33] are easily controlled. Problems associated with competing reactions between matrix interferents and the analyte of interest are largely eliminated with an efficient chromatographic separation.

The potential advantages of IMS as a detector for gas, supercritical fluid, or liquid chromatography are numerous. It is a highly sensitive technique, capable of producing flame ionization detector (FID)-like or ECD-like responses in a nonselective positive ion mode or a nonselective negative ion mode, respectively. Selectivity is achievable by monitoring a specific mobility window. In supercritical fluid chromatography (SFC), its stable ECD-like response under pressure programmed con-

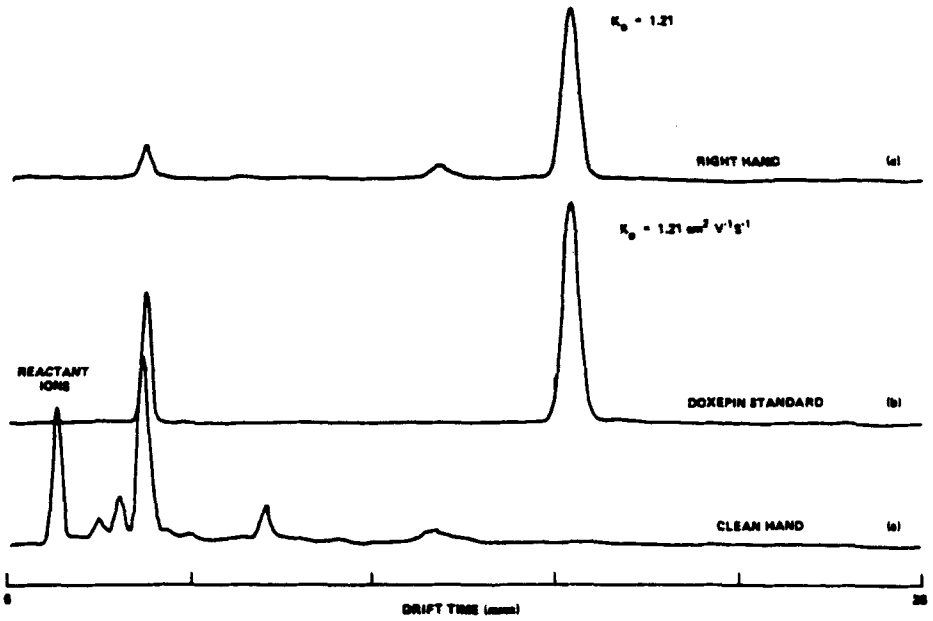

FIGURE 25. Ion mobility spectra obtained from (a) a clean hand, (b) a doxepin standard, (c) the right hand of a patient admitted with a doxepin overdose. (From Lawrence, A. H., *Anal. Chem.*, 58, 1269, 1986. With permission.)

ditions and its potential suitability with numerous modifiers are especially valuable. In liquid chromatography, the corona-spray nubulizer/ionizer potentially extends the range of detection to nonchromophore-containing compounds that are not monitorable by a UV-Vis detector.

A. Gas Chromatography

IMS was first coupled to a gas chromatograph in 1972.[117] Ion mobility spectra of 3 ng samples of musk ambrette were collected. Sensitivity was significantly better than that obtained with a FID. The separation used packed column technology and contamination from column bleed was reported.

The first chromatogram was presented in the literature in 1977.[11] This packed column separation of p-chlorotoluene, 2,4-dichlorotoluene, and 2,4-5-trichlorotoluene is seen in Figure 26. Increased residence times in the detector were noted, and a reduction in the ionization volume was suggested to facilitate sweeping of neutrals from the detector.

The problem of column bleed was addressed more closely in 1978,[118] as the effect of 19 common liquid phases on IMS reactant ions was examined. The positive mode of IMS was found to be extremely sensitive to many stationary phases and was thus somewhat restricted in a choice of columns for use. With the introduction of permanently bonded fused silica capillary columns, this problem has been large circumvented. We have found column bleed from properly conditioned capillary columns to only be a factor when working very near to the producer's suggested temperature limits.

Cognizant of the need to efficiently sweep neutrals from the ionization region, in order to maintain the resolution of capillary gas chromatography, a new detector design was introduced in 1982.[12] Modifications to standard designs included (1) unidirectional gas flow, (2) an enclosed drift tube, (3) a

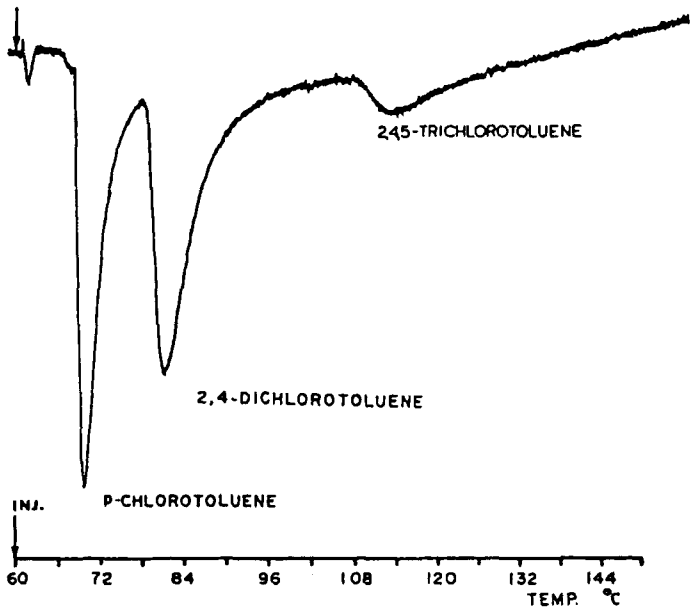

FIGURE 26. Packed column gas chromatography with ion mobility detection. Column; 4 ft × 4 mm I.D., borosilicate, 0.2% carbowax 20 m on Chromosorb W, *100 to 120 mesh, 60 to 150°C at 10°C/min.* Detector; drift gas — 560 ml/min N_2, 140°C, 214 V/cm. (From Karasek, F. W., Hill, H. H., Jr., Kim, S. H., and Rokushika, S., *J. Chromatogr.*, 135, 329, 1977. With permission.)

reduced ionization cell volume, and (4) introduction of samples between the ionization region and the first ion gate. A schematic is illustrated in Figure 3. With this detector, the first high resolution capillary chromatograms were obtained. Figure 27 is a nonselective positive mode chromatogram of orange extract.

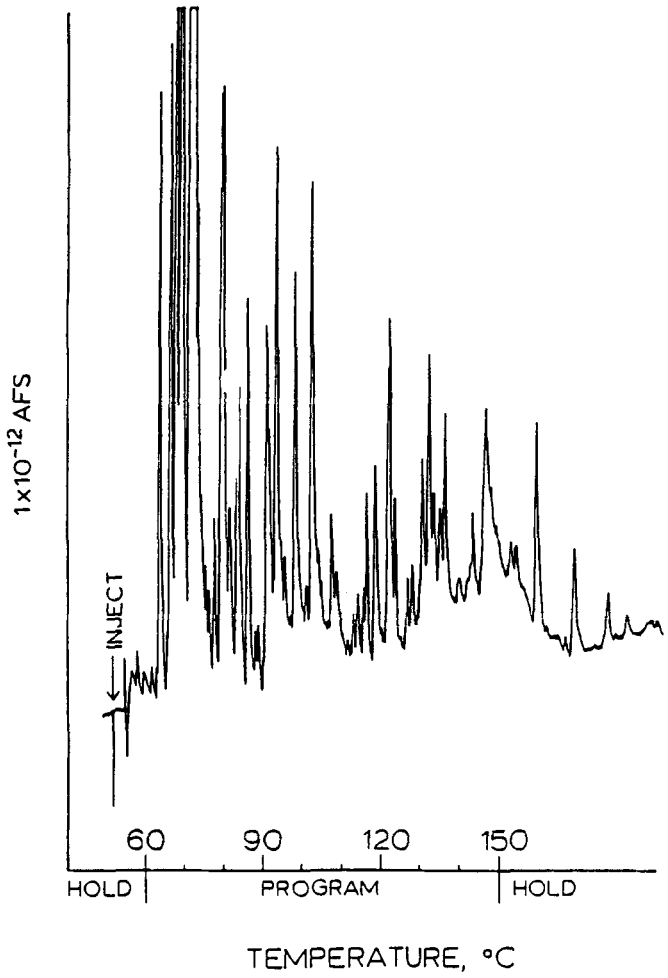

FIGURE 27. Capillary gas chromatography — ion mobility detection, using detector design of 1982, Figure 3. Nonselective chromatogram of orange extract. Column; 15 m, SE-54, 60°C — 2 min, 4°C/min, 150°C — 10 min. Detector; drift gas — 600 ml/min N_2, 155°C, 215 V/cm. (From Baim, M. A. and Hill, H. H., Jr., *J. High Resolution Chromatogr. Chromatogr. Commun.*, 6, 4, 1983. With permission.)

Selective, negative mode capabilities of this detector were demonstrated in 1983 for halogenated species[119] and for quantifying 2,4-dichlorophenoxyacetic acid (2,4-D) residues in soils.[120] Figure 28 compares a FID chromatogram, an ECD chromatogram, and a selective IMD chromatogram for a typical soil sample. Due to the associative electron capture of the 2,4-D methyl ester, as opposed to the more typical dissociative electron capture of chlorinated species, virtually perfect selectivity was obtained by the IMD mobility monitoring. Doping of the drift gas with 0.5% O_2 has been shown to enhance the sensitivity of chlorinated and brominated benzene compounds that respond via a dissociative mechanism.[119] By replacing the Teflon insulators of the detector with glass insulation, it proved suitable for higher temperature separations (300°C) of opiate, acidic analgesic, benzodiazepinone, tricyclic antidepressant,[63] and barbituate[121] extracts from human urine.

A new detector design was again introduced in 1988.[122] Design modifications were directed toward continued improvement in chromatographic resolution and stability. A schematic of the detector is illustrated in Figure 29. Major modifications include (1) a direct axial introduction of the capillary column into the ionization region of the detector; (2) a variable capillary insertion distance, providing a sensitivity/resolution interplay that can be modified dependent on the needs of the assay; (3) a reduction in ionization cell volume to 0.8 cm^3; and (4) an inert gas flow external to the drift cylinder, preventing atmospheric impurities from infiltrating the detector.

The capabilities of the system are evidenced by Figures 30 through 32, gas chromatograms of orange extract, petroleum ether, and a commercial perfume. Several additional chromatograms of complex samples are presented in a recent review of ion mobility detection after capillary gas chromatography.[123] Continued improvement in the use of IMS as a detector for gas chromatography is readily apparent by comparing the packed column chromatogram of 1977 (Figure 26), the orange extract chromatogram using the design of 1982 (Figure 27), and the chromatograms from the design of 1988 (Figures 30 through 32).

Initial studies with the design of 1988 addressed previously reported inadequacies of IMS for the qualitative and quantitative detection of ethers. An earlier work,[33] using a traditional bidirectional flow IMS and direct injection of microgram quantities of ethers into the ionization source, reported spectral instabilities in drift times and intensities, with residence times exceeding 1.7 h. The recent data, with GC sample introduction of nanogram quantities of ethers, reported stable spectra, an exponential response over greater than two orders of magnitude, and residence times of seconds. The earlier reported difficulties appear to be problems related to experimental and instrumental design, i.e., the sample was present in severely overloaded amounts of questionable purity, and the instrument displayed inefficient sweeping characteristics.

Minimum detectable limits (MDL) obtained were 100 fg/s for tributylamine and diphenylsulfide. The MDL for tributylphosphate was 200 fg/s.[46] These values are roughly an order of magnitude better than those reported for a FID or a flame photometric detector (FPD), and roughly equivalent to those reported for a thermionization detector (TID).[124] Noise measured was 2.0×10^{-14} A. Current work is directed toward determining the applicability of ion mobility detection for microbore (<100 μm I.D.) gas chromatography. It would appear to be ideally suited for detection after microbore GC as the needs of microbore GC emphasize IMS's primary strength,

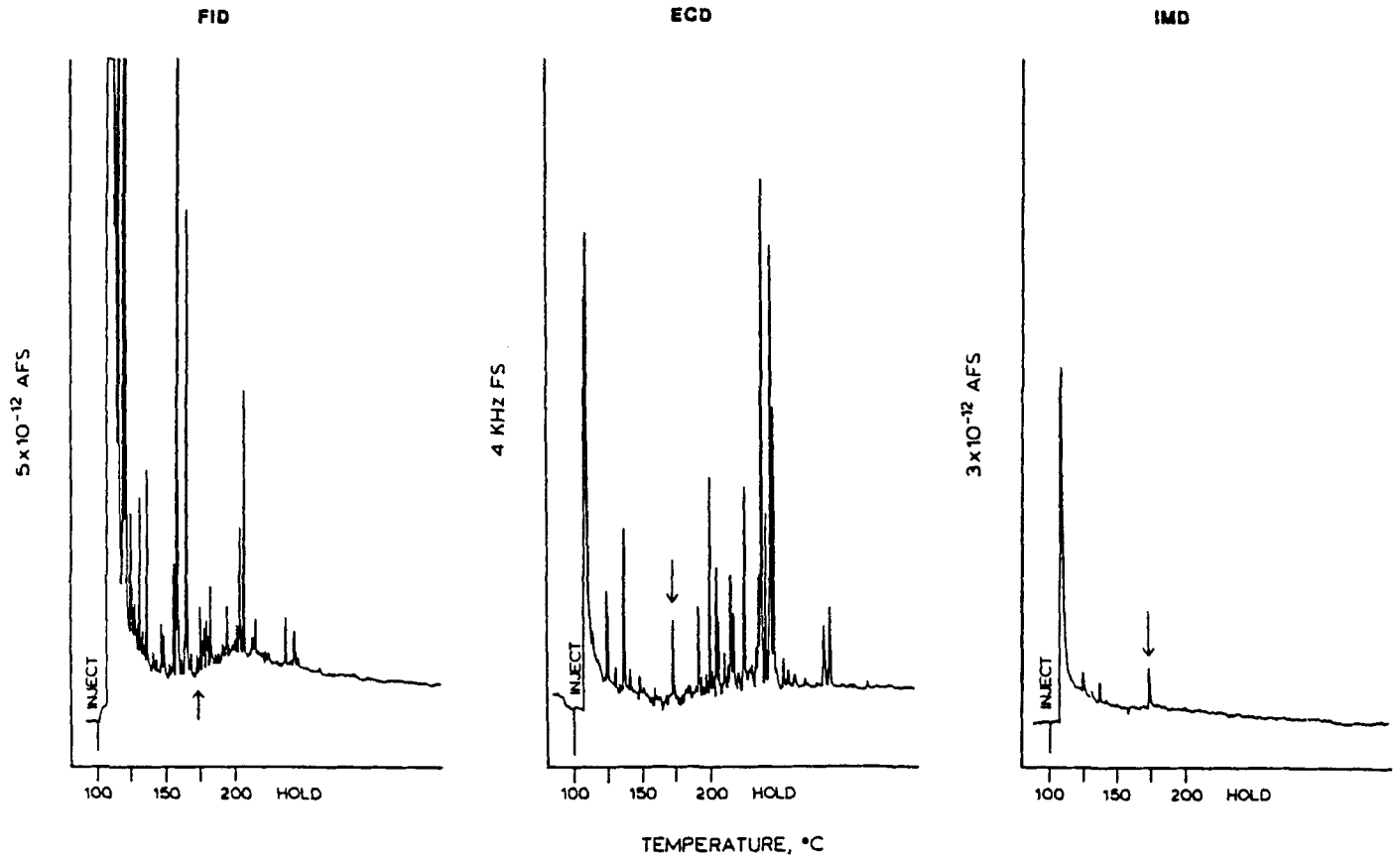

FIGURE 28. Comparison of FID, ECD, and IMD detector responses to a soil sample. The arrow denotes the retention time of 2,4-D methyl ester. (From Baim, M. A. and Hill, H. H., Jr., *J. Chromatogr.*, 279, 631, 1983. With permission.)

ultrasensitivity, and minimize its primary weakness, limited linear range.

B. Supercritical Fluid Chromatography

SFC has been found to be compatible with a wide variety of detection methods commonly used in liquid or gas chromatography. For quantitative information the most common detectors in SFC are the UV-Vis absorption detector and the FID. For qualitative information, FTIR and mass spectrometry are being investigated.

Unfortunately, each of these detection methods is limited to specific conditions. The UV-Vis detector is limited to chromophore-containing analyte compounds and nonabsorbing mobile phases. The FID is limited to the use of mobile phases which do not contain ionizable species. FTIR is limited to mobile phases not absorbing in the information-rich region of the spectra. MS is limited in the molecular weight that can be detected, and both MS and FTIR are costly. A common situation in SFC is that detector requirements rather than separation requirements determine the chromatographic conditions. Recent work demonstrates IMS to be a sensitive detection method under a variety of SFC conditions.

The first attempts to interface SFC to IMS used the standard two-directional flow ion mobility spectrometer.[13,125] With this ion mobility spectrometer, it was found that, because of the two directional nature of its flow design, considerable mixing of the CO_2 mobile phase and N_2 drift gas occurred producing reactant ions that varied with pressure. CO_2 was consequently investigated as the IMS drift gas. Product ions from a series of fatty acid methylesters displayed considerably lower mobilities in CO_2 than in N_2. These mobilities increased with temperature suggestive of a clustering phenomena, i.e., as the temperature increases, the average size of the cluster decreases, and the mobility increases. The IMS sensitivity was significantly better than that observed by a UV-Vis detector at 210 nm.[125] Solvent clearance times of greater than 30 min were reported.

Using a unidirectional flow IMD (described in gas chromatography section), difficulties with N_2 as the drift gas and excessive residence times were eliminated.[126] Figure 33 demonstrates the effect that the CO_2 mobile phase had on the reactant ions when using a bidirectional flow IMS. Figure 34 shows the results from a similar experiment using the unidirectional flow detector. Note that, with the unidirectional flow design, reactant ions were unchanged when CO_2 was introduced into the detector. More importantly, agreement was ob-

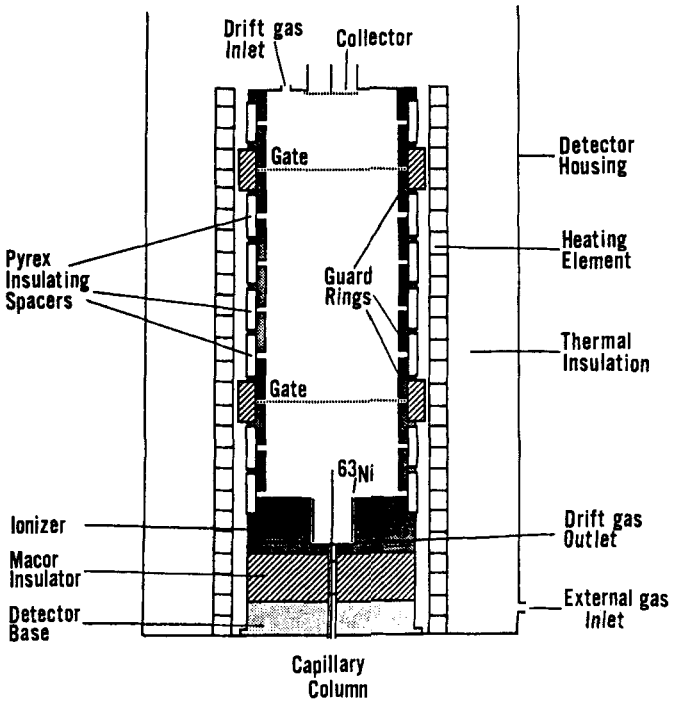

FIGURE 29. Ion mobility detector for capillary gas chromatography. Note, direct introduction of capillary column into ionization region. (From St. Louis, R. H., Siems, W. F., and Hill, H. H., Jr., *J. Chromatogr.*, 479, 221, 1989. With permission.)

tained from mobility values of testosterone, esterone, progesterone, diazepam, nitrazepan, and flurazepan when compared after introduction by capillary GC and capillary SFC.[127]

The potential utility of IMS with several ionizable modifiers was recently demonstrated.[14] A stable baseline response was evidenced in both the positive and negative modes using methanol, acetone, methylene chloride, dichlorodifloromethane, and dichlorofloromethane modified CO_2 as the SFC mobile phase under pressure programming conditions.

An ECD-like response was demonstrated for 15 chlorinated pesticides.[128] Figure 35 is a SFC chromatogram of 10 of those pesticides obtained with negative mode ion mobility detection using a unidirectional flow detector. The ECD chromatogram under similar pressure programmed conditions is illustrated in Figure 36. Other applications of IMS after SFC include the sensitive and selective detection of 2,4-D, cholesterols and cholesterol esters, di- and triglycerides, and polydimethylsilicone oligomers.[129] Individual methylsilicone oligomers of greater than 3000 amu were detected. A more complete review of IMS as a detection method for SFC is available.[130]

C. Liquid Chromatography

IMS was first evaluated as a detector for liquid chromatography in 1973.[131] The sample was introduced with the moving-wire technique illustrated in Figure 37. The method involves wetting the surface of a wire with a thin film of column effluent.

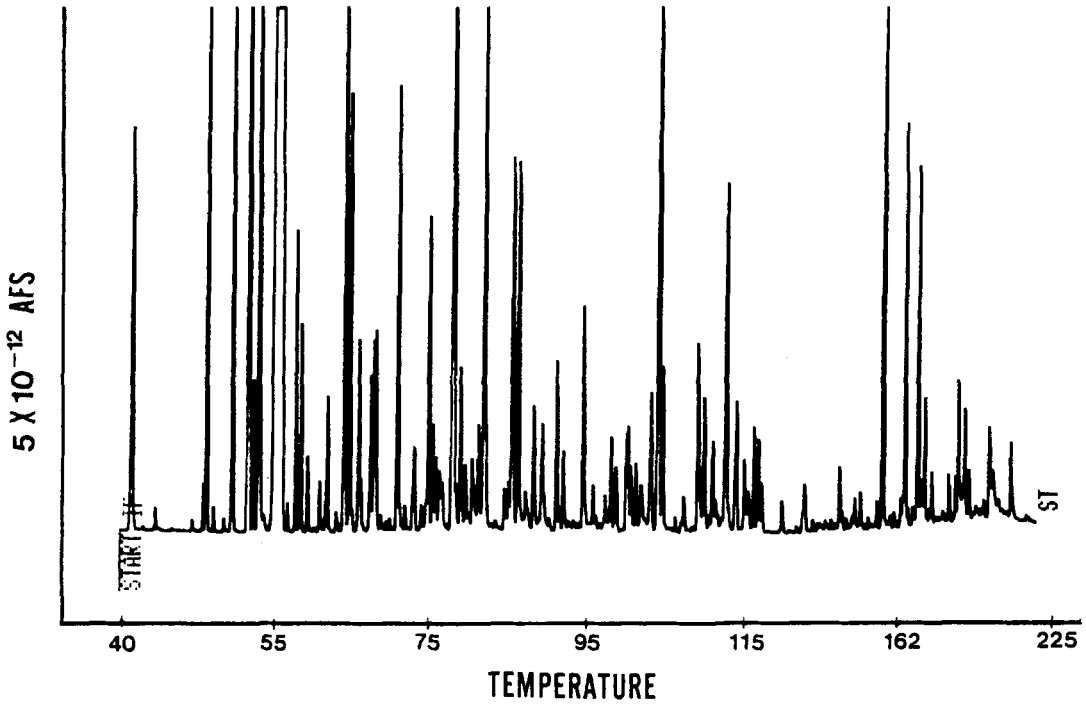

FIGURE 30. Capillary gas chromatography — ion mobility detection using detector design of 1988. Nonselective chromatogram of orange extract. Column; 22 m, DB-5, 40°C — 5 min, 1°C/min, 120°C — 1 min, 3°C/min, 150°C — 1 min, 5°C/min, 225°C — 5 min. Detector; drift gas — 1400 ml/min air, 200°C, 340 V/cm.

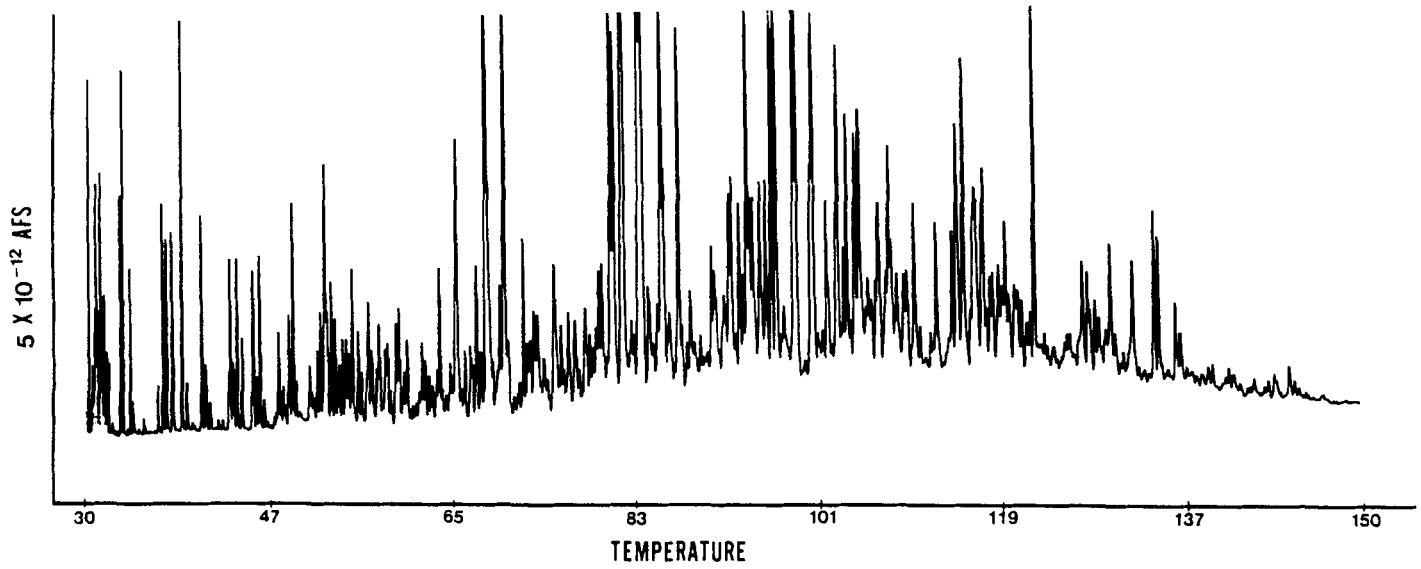

FIGURE 31. Nonselective chromatogram of petroleum ether. Column; 22 m, DB-5, 30°C — 1 min, 0.6°C/min, 150°C — 5 min. Detector; 1400 ml/min air, 200°C, 340 V/cm.

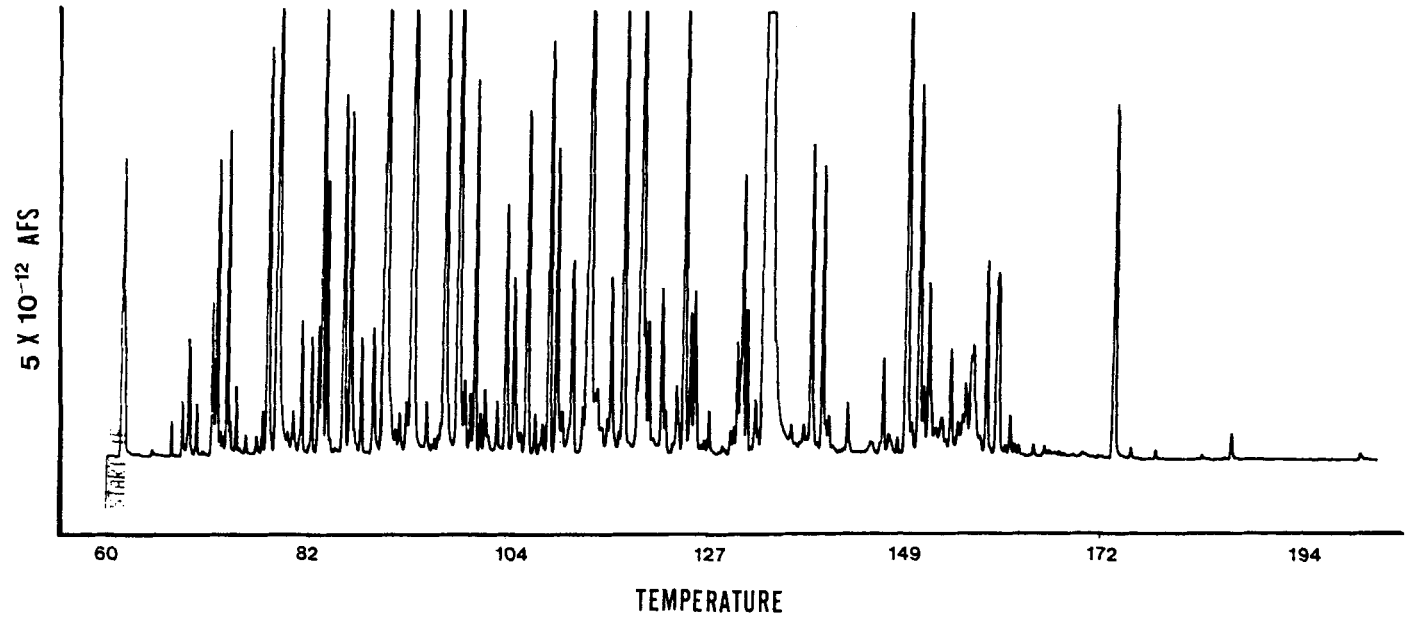

FIGURE 32. Chromatogram of White Linen fragrance. Column; 22 m, DB-5, 60°C — 1 min, 1.5°C/min, 200°C — 5 min. Detector; 1400 ml/min air, 225°C, 340 V/cm.

The solvent is allowed to evaporate and the sample coated wire is then momentarily inserted into the heated inlet of an ion mobility spectrometer. Spectra were successfully obtained for halogenated benzenes, DDT, Endrin, and Dieldrin. Spectral collection times approximated 2 min, and no chromatograms were shown.

Current studies are evaluating the direct interfacing of liquid chromatography and IMS using electrified spray nebulization and ionization. The first ion mobility spectrum obtained for an organic with electrified spray was of lysozyme in an ethanol solvent.[104] This was followed by attempts to separate oligomers of electrosprayed polystyrene and polyvinylpyrolidine.[100] Results were less than satisfactory due to the limited resolution of the system. This low resolution is possibly attributable to inefficient sweeping of neutrals out of the system, leading to ion-molecule reactions in drift region, or to incomplete evaporation of the solvent prior to entering the drift region. Investigations in the authors' laboratory attempted to solve these

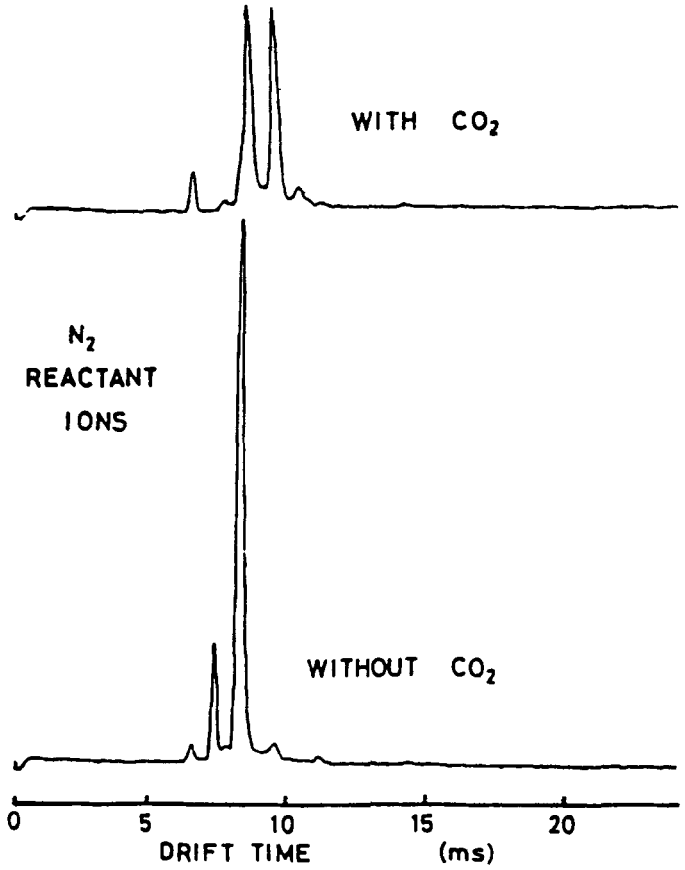

FIGURE 33. Bidirectional flow IMS used as a detector after supercritical fluid chromatography. Note changes in reactant ion spectrum as CO_2 is introduced from SFC column.

problems using a unidirectional flow ion mobility detector. Early results are encouraging. Figure 38 shows an electrified spray ion mobility liquid chromatogram.[132] It is a separation of approximately 10 ng of methylparaben, propylparaben, and butylparaben.

The unidirectional flow, electrified spray ion mobility spectrometer is also being evaluated as a detector following capillary zone electrophoresis (CZE). Figure 39 is a schematic of the CZE-IMS system. One end of the capillary is momentarily placed in a vial containing the sample and a suitable buffer. A small plug of sample enters the capillary which is then inserted into a vial containing buffer only. An electrophoretic separation occurs in the capillary column which is directly interfaced to the ion mobility spectrometer. Figure 40 illustrates the background reactant ions with only phosphate buffer present, pH 7.0. The depletion of reactant ions and formation of product ions are seen as tetramethyl ammonium iodide and tetrabutyl ammonium iodide are introduced into the system.

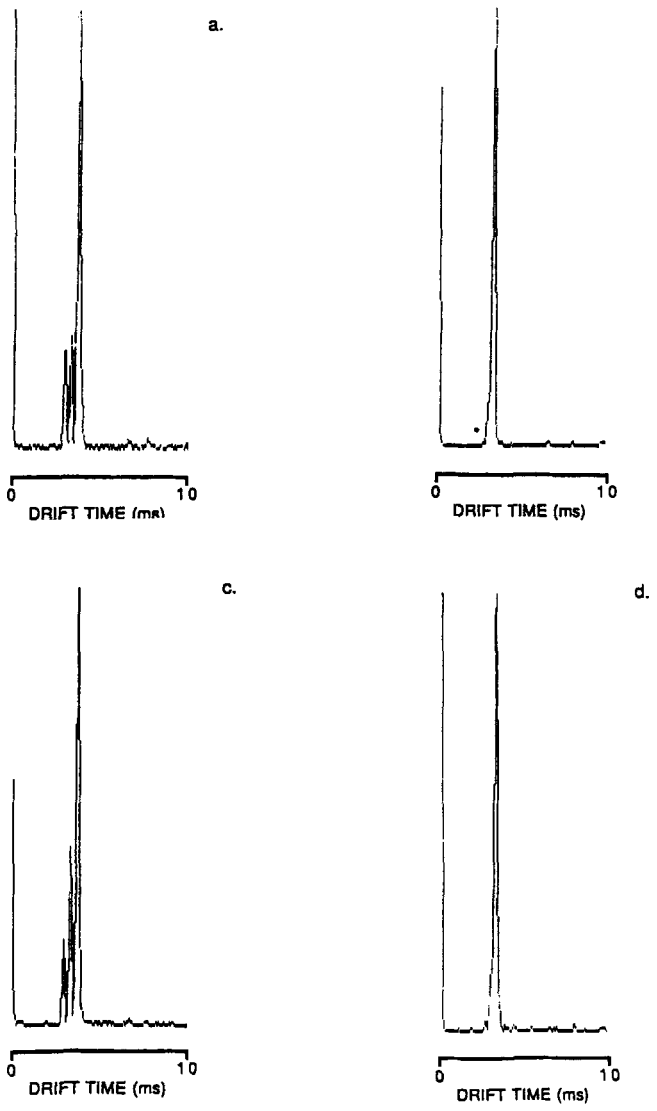

FIGURE 34. Unidirectional flow IMS used as a detector after supercritical fluid chromatography. (a) Positive mode reactant ions, CO_2 flow, 2 ml/min. (b) Negative mode reactant ions, CO_2 flow, 2 ml/min. (c) Positive mode reactant ions, no CO_2 flow. (d) Negative mode reactant ions, no CO_2. Note that reactant ion spectrum is essentially unchanged.

X. CONCLUSIONS AND FUTURE DIRECTIONS

No matter how you calculate IMS efficiency, IMS is a low resolution ion separation technique. In chromatographic terms, it has a plate number of around 5000; in mass spectrometric terms, it has a peak position/peak width ratio of about 30; and in electrophoretic terms, it can separate mobilities which differ by more than about 0.2%. Because it is a gas phase ion sep-

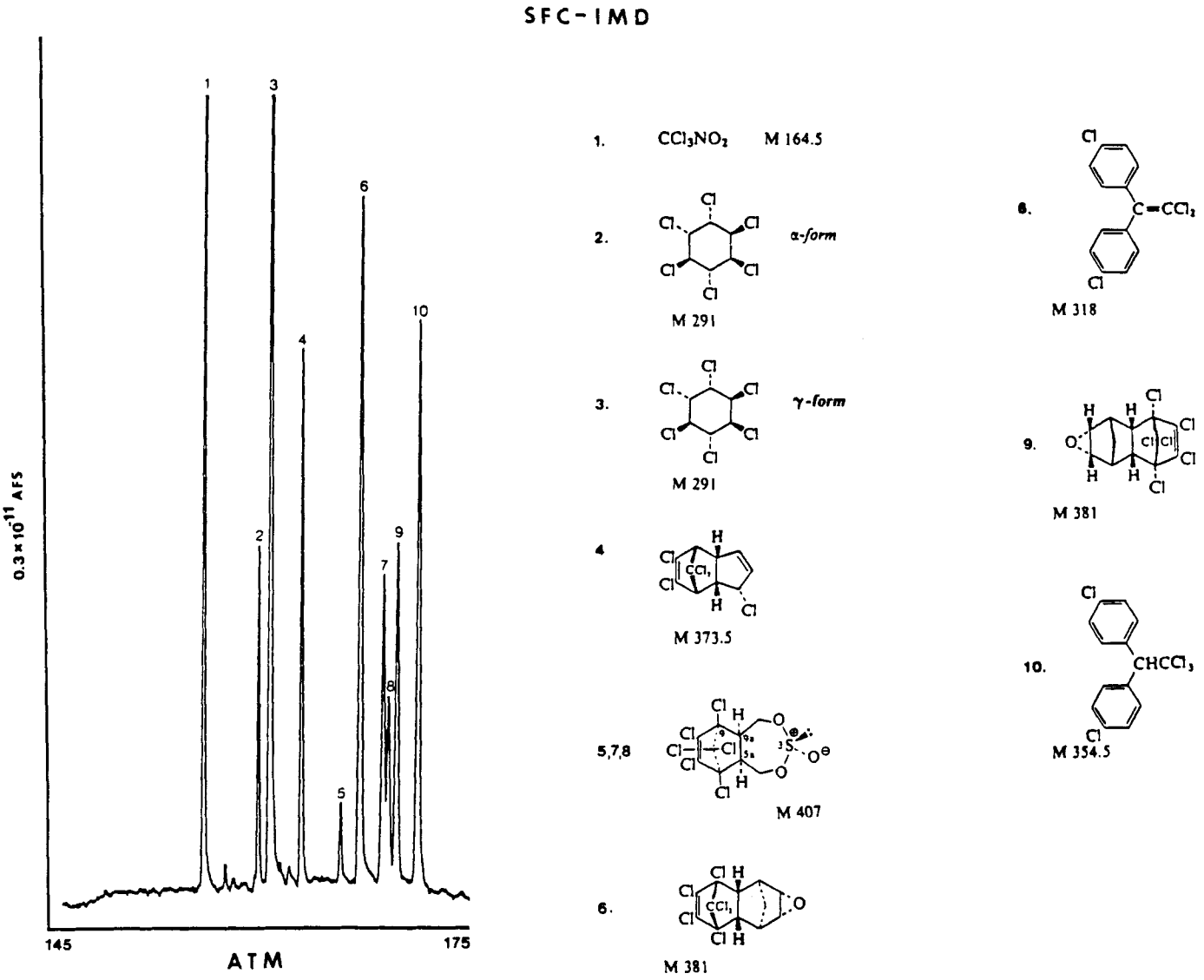

FIGURE 35. Negative ion mobility detection of chlorinated pesticides after pressure programmed supercritical fluid chromatography.

aration technique, it is often compared to mass spectrometry which is unfortunate because it is a low resolution instrument and, at best, it provides only approximate mass information. Its unique advantages relative to mass spectrometry rest only in that it is an atmospheric pressure device and that in many cases it can provide structural information for isomers. As a general analytical tool, however, it is better to compare IMS to UV-Vis absorption spectrometry rather than mass spectrometry.

Although the mechanism of response is different, the quantity of information provided by an ion mobility spectrum is similar to that of a UV-Vis spectrum. As with UV-Vis spectrometry, IMS is best suited for the analysis of simple mixtures in which the content of the mixture is well known or of complex mixtures after component separation. Because IMS is a gas phase ionization technique rather than a light absorption technique, the quality of information is complimentary to UV-Vis spectrometry, providing analytical information on compounds which do not contain chromaphors and do not contain large molar absorptivities. Thus, we see IMS developing as an analytical technique, taking its place alongside UV-Vis spectrometry as a detection method for well-defined systems such as in process control applications and flow injection analyses and as a detection method after chromatographic separation of complex mixtures.

ACKNOWLEDGMENT

This work was supported in part by a grant from the Public Health Service (GM29523).

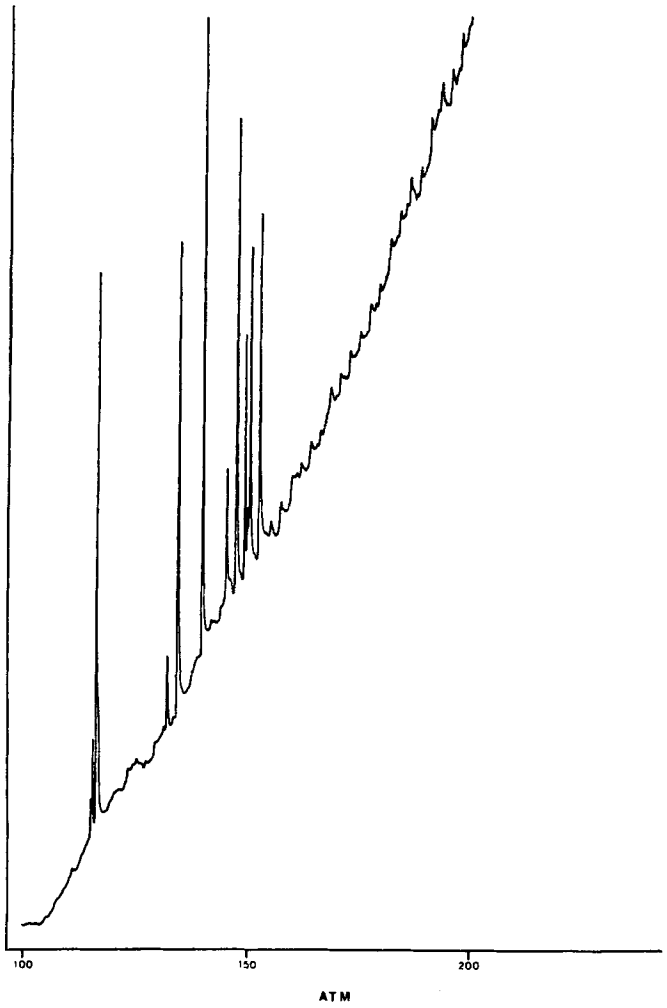

FIGURE 36. Electron capture detection after pressure programmed supercritical fluid chromatography. Baseline instabilities limit usefulness of ECD under pressure programmed conditions.

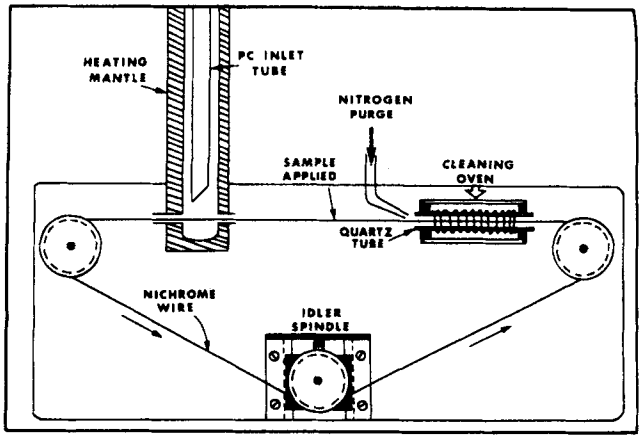

FIGURE 37. Schematic of moving wire sample introduction. (From Karasek, F. W. and Denny, D. W., *Anal. Lett.*, 6(11), 993, 1973. With permission.)

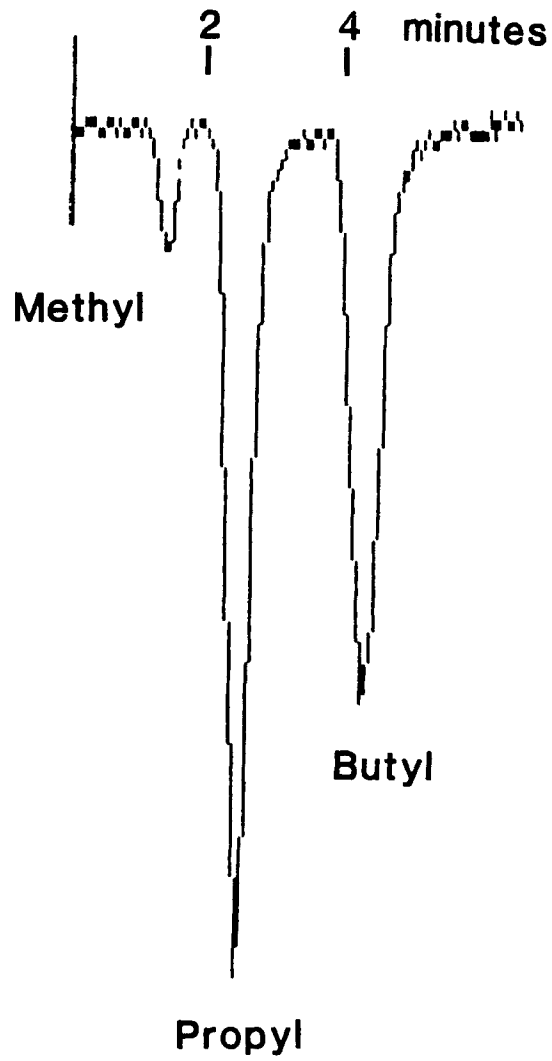

FIGURE 38. Coronaspray ionization-ion mobility detection after liquid chromatography. Chromatographic separation of methylparaben, propylparaben, and butylparaben.

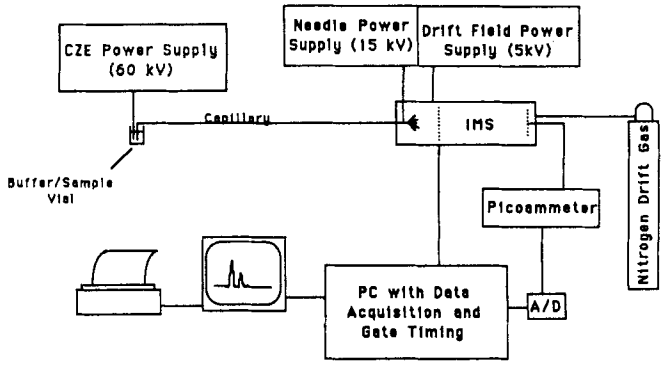

FIGURE 39. Schematic of capillary zone electrophoresis-electrified spray-ion mobility spectrometry system.

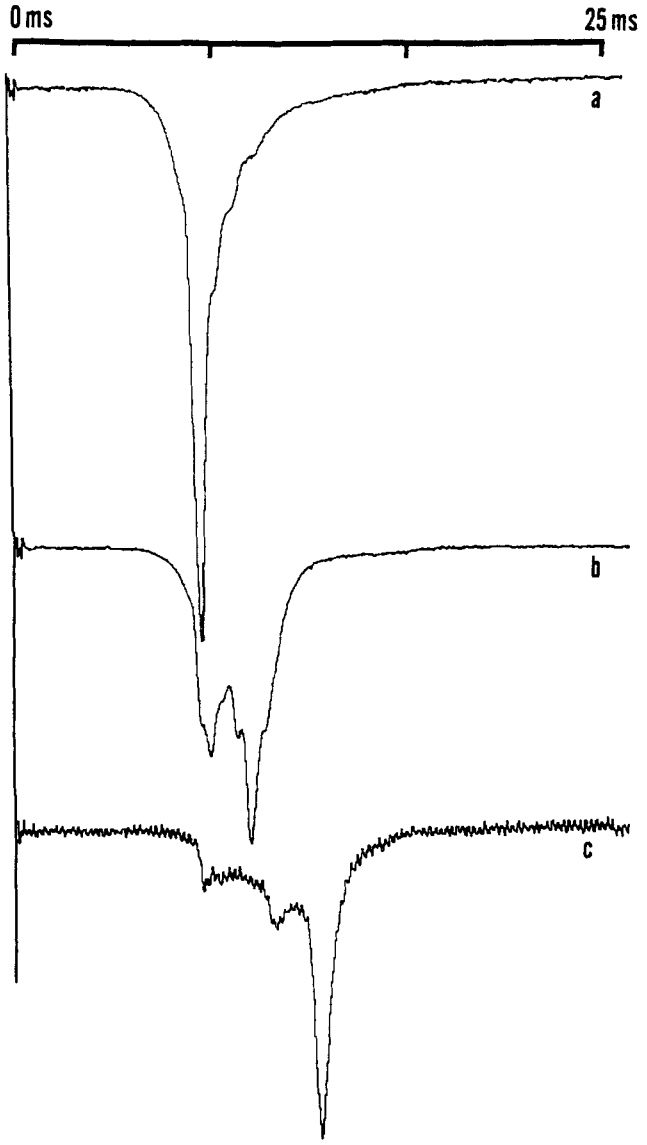

FIGURE 40. Representative spectra obtained after capillary zone electrophoresis. (a) Background reactant ions. (b) Product ions, tetramethyl ammonium iodide. (c) Product ions, tetrabutyl ammonium iodide.

LIST OF SYMBOLS

A	=	Analyte molecule.
A^+	=	Positive analyte ion.
A^-	=	Negative analyte ion.
A_m	=	Cross-sectional area of a membrane.
α	=	Correction factor in mobility equation.
AB	=	Analyte molecule.
AB*	=	Excited analyte molecule.
β	=	Beta particle.
β'	=	Beta particle of reduced energy.
2b	=	Height of a guard ring.
C	=	Third body molecule.
C_A	=	Activity of a radioactive source.
C(A)	=	Concentration of molecule A.
c	=	Radius of a guard ring.
D	=	Diffusion coefficient of an ion.
D_a	=	Diffusion coefficient of the ion A^+.
d	=	Sum of ion and drift gas radii.
E	=	Electric field.
ΔE	=	Distortion of electric field.
e	=	Charge on an electron.
e^-	=	Electron.
ϵ	=	Energy of collision.
F	=	Faraday's constant.
F_c	=	Carrier gas flow rate.
F[]	=	Function of [].
2f	=	Gap separating guard rings.
γ	=	Gamma energy.
H	=	Membrane thhickness.
h	=	Distance between the gaps of successive guard rings.
$\hbar$	=	Planck's constant.
I°	=	Electromagnetic radiation with no absorbing species present.
I	=	Transmitted radiation.
I(A)	=	Measured ion intensity of a peak corresponding to molecule A.
i	=	Measured ion current.
i_o	=	Total ion current of the system.
K	=	Mobility of an ion.
K_o	=	Reduced mobility of an ion, corrected for pressure and temperature.
K_R	=	Generic recombination rate constant.
K_{R1-3}	=	Positive-negative recombination rate constants.
K_+	=	Reactant ion-analyte molecule formation rate constant.
K_{2-7}	=	Reaction rate constants.
k	=	Boltzmann's constant.
L	=	Photo-path length.
l_d	=	Drift length.
m	=	Mass of an ion.
M	=	Mass of neutral drift gas molecule.
N	=	Number density of the drift gas.
N_L	=	Loschmidt number (2.69×10^{19} molecules/cm^3).
N_o	=	Avagadro's number.
n_o	=	Ions per unit area admitted through entrance gate.
n	=	Ions per unit area.
η	=	Photoionization efficiency.
Ω_D	=	Ion-neutral cross section.
P	=	Atmospheric pressure.
P_I	=	Partial pressure of analyte molecule interior to a membrane inlet.
P_R	=	Permeability coefficient of a membrane.

P_x	=	Partial pressure of analyte molecule exterior to a membrane inlet.
q	=	Ionic charge.
Q_D	=	Integral involved in derivation of Ω_D, concerned with collision energy and scattering angle.
R	=	Experimentally measured resolution.
R_d	=	Diffusion controlled resolution.
R^+	=	Positive reactant ion.
R^-	=	Negative reactant ion.
$[R_o^+]$	=	Positive reactant ion concentration with no analyte molecules present.
R_{1-6}	=	Reaction rates.
r	=	Radial distance.
S	=	Reactant ion pairs formed per second per unit volume.
s	=	Differential cross section for scattering.
$S_{1/2}$	=	Half-height spatial width of a Gaussian peak.
σ	=	Absorption cross section of a molecule.
T	=	Kelvin temperature.
$T_{1/2}$	=	Measured peak width at half height.
T_s	=	Spectral collection time.
t	=	Time.
t_d	=	Drift time.
t_o	=	Half-width of initial ion pulse.
$t_{1/2}$	=	Diffusion controlled half-width.
t_x	=	Portion of half-width measurement not due to initial pulse width or diffusion.
θ	=	Scattering angle.
μ	=	Reduced mass.
V	=	Applied voltage.
V_N	=	Volume of 1 mol of gas at stp.
V_s	=	Ion source volume.
v_d	=	Drift velocity.
ν	=	Frequency of electromagnetic radiation.
W	=	Mean β-ray energy per disintegration.
x	=	Drift distance.
x_d	=	Drift distance of the center of a Gaussian ion pulse.
$\langle X^2 \rangle$	=	Mean square distance from all points in the source volume to the walls.
z	=	Unit ionic charge.

REFERENCES

1. **Karasek, F. W.,** The plasma chromatograph, *Res. Dev.*, 21, 34, 1970.
2. **Cohen, M. J. and Karasek, F. W.,** Plasma chromatography — a new dimension for gas chromatography and mass spectroscopy, *J. Chromatogr. Sci.*, 8, 330, 1970.
3. **Karasek, F. W. and Kane, D. M.,** Plasma chromatography of the n-alkyl alcohols, *J. Chromatogr. Sci.*, 10, 673, 1972.
4. **Karasek, F. W., Tatone, O. S., and Denney, D. W.,** Plasma chromatography of the n-alkyl halides, *J. Chromatogr.*, 87, 137, 1973.
5. **Karasek, F. W., Tatone, O. S., and Kane, D. M.,** Study of electron capture behavior of substituted aromatics by plasma chromatography, *Anal. Chem.*, 45, 1210, 1973.
6. **Karasek, F. W., Denney, D. W., and Dedecker, E. H.,** Plasma chromatography of normal alkanes and its relationship to chemical ionization mass spectrometry, *Anal. Chem.*, 46, 970, 1974.
7. **Karasek, F. W. and Denney, D. W.,** Detection of aliphatic N-nitrosamine compounds by plasma chromatography, *Anal. Chem.*, 46, 1312, 1974.
8. **Karasek, F. W., Maican, A., and Tatone, O. S.,** Plasma chromatography of n-alkyl acetates, *J. Chromatogr.*, 110, 295, 1975.
9. **Karasek, F. W., Kim, S. H., and Rokushika, S.,** Plasma chromatography of alkyl amines, *Anal. Chem.*, 50, 2013, 1978.
10. **Spangler, G. E. and Lawless, P. A.,** Ionization of nitrotoluene compounds in negative ion plasma chromatography, *Anal. Chem.*, 50, 884, 1978.
11. **Karasek, F. W., Hill, H. H., Jr., Kim, S. H., and Rokushika, S.,** Gas chromatographic detection modes for the plasma chromatograph, *J. Chromatogr.*, 135, 329, 1977.
12. **Baim, M. A. and Hill, H. H., Jr.,** Tuneable selective detection for capillary gas chromatography by ion mobility monitoring, *Anal. Chem.*, 54, 38, 1982.
13. **Rokushika, S., Hatano, H., and Hill, H. H., Jr.,** Ion mobility spectrometry in carbon dioxide, *Anal. Chem.*, 58, 361, 1986.
14. **Morrissey, M. A., Tarver, E., and Hill, H. H., Jr.,** Mobile phase modifiers for supercritical fluid chromatography, NW ACS Convention, Spokane, 1988.
15. **Baim, M. A., Eatherton, R. L., and Hill, H. H., Jr.,** Ion mobility detector for gas chromatography with a direct photoionization source, *Anal. Chem.*, 55, 1761, 1983.
16. **Lubman, D. M. and Kronick, M. N.,** Plasma chromatography with laser-produced ions, *Anal. Chem.*, 54, 2289, 1982.
17. **Shumate, C. and Hill, H. H., Jr.,** *Anal. Chem.*, 61, 601, 1989.
18. **Wohltzer, H.,** U.S. Patent Appl. US 581398, AO, 3 August, 1984.
19. **Kim, S. H., Karasek, F. W., and Rokushika, S.,** Plasma chromatography with ammonium reactant ions, *Anal. Chem.*, 50, 152, 1978.
20. **Spangler, G. E., Campbell, D. N., and Carrico, J. P.,** Acetone reactant ions for ion mobility spectrometry, Pittsburgh Conf., Anal. Chem. Appl. Spectrom., Atlantic City, NJ, 1983.
21. **Proctor, C. J. and Todd, J. F. J.,** Alternative reagent ions for plasma chromatography, *Anal. Chem.*, 56, 1794, 1984.
22. **Carr, T. W. and Needham, C. D.,** Analysis of organic surface contamination by plasma chromatography — mass spectroscopy, in *Surface Contamination*, Mittal, K. L., Ed., Plenum Press, New York, 1979.
23. **Kolaitis, L. and Lubman, D. M.,** Detection of nonvolatile species by laser desorption atmospheric pressure mass spectrometry, *Anal. Chem.*, 58, 2137, 1986.
24. **Spangler, G. E. and Carrico, J. P.,** Membrane inlet for ion mobility spectrometry, *Int. J. Mass Spectrom. Ion Phys.*, 52, 267, 1983.
25. **Dam, R. J.,** Analysis of toxic vapors by plasma chromatography, in *Plasma Chromatography*, Carr, T., W., Ed., Plenum Press, New York, 1984.
26. **Carrico, J. P., Davis, A. W., Campbell, D. N., Roehl, J. E., Sima, G. R., Spangler, G. E., Vora, K. N., and White, R.J.,** Chemical detection and alarm for hazardous chemicals, *Am. Lab.*, February, 152, 1986.
27. **Roehl, J. E.,** Microprocessor controlled chemical detection and alarm system based on ion mobility spectrometry, *Opt. Eng.*, 24, 985, 1985.
28. **Knorr, F. J., Eatherton, R. L., Siems, W. F., and Hill, H. H., Jr.,** Fourier transform ion mobility spectrometry, *Anal. Chem.*, 57, 402, 1985.
29. **Carr, T. W., Ed.,** *Plasma Chromatography*, Plenum Press, New

York, 1984.
30. **Spangler, G. E., Campbell, D. N., Vora, K. N., and Carrico, J. P.,** Developments in ion mobility spectrometry, *ISA Trans.*, 23, 17, 1984.
31. **Carrico, J. P., Sickenberger, D. W., Spangler, G. E., and Vora, K. N.,** Simple electrode design for an ion mobility spectrometer, *J. Phys. E. Sci. Instrum.*, 16, 1058, 1983.
32. **Spangler, G. E. and Cohen, M. J.,** Instrument design and description, in *Plasma Chromatography,* Carr, T. W., Ed., Plenum Press, New York, 1984, 1.
33. **Metro, M. M. and Keller, R. A.,** Fast scan ion mobility spectra of diethyl, dipropyl, and dibutyl ethers as determined by the plasma chromatograph, *J. Chromatogr. Sci.*, 11, 520, 1973.
34. **O'Keefe, A. E. and Ortman, G. C.,** Primary standards for trace gas analysis, *Anal. Chem.*, 38, 760, 1966.
35. **Grob, R. L., Ed.,** *Modern Practice of Gas Chromatography,* John Wiley & Sons, New York, 1977, 194.
36. **Nanji, A. A., Lawrence, A. H., and Mikhael, N. Z.,** Use of skin surface sampling and ion mobility spectrometry as a preliminary screening method for drug detection in an emergency room, *Clin. Toxicol.*, 25, 501, 1987.
37. **Huang, S. D., Kolaitis, L., and Lubman, D. M.,** Detection of explosives using laser desorption in ion mobility spectrometry/mass spectrometry, *Appl. Spectrosc.*, 41, 1371, 1987.
38. **Spangler, G. E. and Collins, C. I.,** Reactant ions in negative ion plasma chromatography, *Anal. Chem.*, 47, 393, 1975.
39. **Youngquist, G. R.,** *Flow through Porous Media,* Nunje, R. T., Ed., ACS, Washington, D.C., 1970.
40. **Stannett, V., Szware, M., Bhargava, B. L., Meyer, J. A., Myers, A. W., and Rogers, C. E.,** *TAPPI Monogr. Ser.*, 23, 1962.
41. **Spangler, G. E.,** The plasma chromatograph: an atmospheric pressure chemical ionization drift time spectrometer, *Am. Lab.*, 7, 36, 1975.
42. **Spangler, G. E., Carrico, J. P., and Campbell, D. N.,** Recent advances in ion mobility spectrometry for explosives vapor detection, *J. Test. Eval.*, 13, 234, 1985.
43. **Tyndall, A. M.,** *The Mobility of Positive Ions in Gases,* Cambridge University Press, Cambridge, England, 1938.
44. **Bradbury, N. E. and Neilson, R. A.,** Absolute values of the electron mobility in hydrogen, *Phys. Rev.*, 49, 388, 1936.
45. **Aronson, E. A.,** An analysis of ion spectrometry, Sandia National Laboratories Report, SAND87-0072•UC-32, March, 1987.
46. **Siems, W. F., St. Louis, R. H., and Hill, H. H., Jr.,** unpublished data.
47. **Eiceman, G. A.,** New Mexico State University, personal communication.
48. **McDaniel, E. W. and Mason, E. A.,** *The Mobility and Diffusion of Ions in Gases,* Wiley-Interscience, New York, 1973.
49. **Revercomb, H. E. and Mason, E. A.,** Theory of plasma chromatography/gaseous electrophoresis — a review, *Anal. Chem.*, 47, 970, 1975.
50. **Mason, E. A.,** Ion mobility: its role in plasma chromatography, in *Plasma Chromatography,* Carr, T. W., Ed., Plenum Press, New York, 1984, 43.
51. **Griffin, G. W., Dzidic, I., Carroll, O. I., Stillwell, R. N., and Horning, E. C.,** Ion mass assignments based on mobility measurements, *Anal. Chem.*, 45, 1204, 1973.
52. **Kim, S. H.,** Ph.D. dissertation, University of Waterloo, Ontario, 1977.
53. **Karasek, F. W. and Kane, D. M.,** Plasma chromatography of isomeric halogenated nitrobenzenes, *Anal. Chem.*, 46, 780, 1974.
54. **Karasek, F. W. and Kim, S. H.,** Identification of the isomeric phthalic acids by mobility and mass spectra, *Anal. Chem.*, 47, 1166, 1975.
55. **Carr, T. W.,** Analysis of surface contaminants by plasma chromatography — mass spectroscopy, *Thin Solid Films,* 45, 115, 1977.
56. **Hagen, D. F.,** Characterization of isomeric compounds by gas and plasma chromatography, *Anal. Chem.*, 51, 870, 1979.
57. **Karpas, Z., Stimac, R. M., and Rappoport, Z.,** Differentiating between large isomers and derivation of structural information by ion mobility spectrometry/mass spectrometry techniques, *Int. J. Mass Spectrom. Ion Proc.*, 83, 163, 1988.
58. **Karpas, Z., Cohen, M. J., Stimac, R. M., and Wernlund, R. F.,** On the effects of structure and charge distribution on the mobility of ions, *Int. J. Mass Spectrom. Ion Proc.*, 74, 153, 1986.
59. **Karpas, Z.,** Ion mobility spectrometry of aliphatic and aromatic amines, *Anal. Chem.*, 61, 684, 1989.
60. **Shumate, C., St. Louis, R. H., and Hill, H. H., Jr.,** Table of reduced mobility values from ambient pressure ion mobility spectrometry, *J. Chromatogr.*, 373, 141, 1986.
61. **Lubman, D. M.,** Temperature dependence of plasma chromatography of aromatic hydrocarbons, *Anal. Chem.*, 56, 1298, 1984.
62. **Perent, D. C. and Bowers, M. T.,** Temperature dependence of ion mobilities: experiment and theory, *Chem. Phys.*, 60, 257, 1981.
63. **Eatherton, R. L.,** Ph.D. thesis, Washington State University, Pullman, WA, 1987.
64. **Kolaitis, L. and Lubman, D. M.,** Atmospheric pressure ionization mass spectrometry with laser-produced ions, *Anal. Chem.*, 58, 1993, 1986.
65. **Wannier, G. H.,** Motion of gaseous ions in strong electric fields, *Bell Syst. Tech. J.*, 32, 170, 1953.
66. **Baim, M. A.,** Ph.D. thesis, Washington State University, Pullman, WA, 1984.
67. **Rokushika, S., Hatano, H., Baim, M. A., and Hill, H. H., Jr.,** Resolution measurement for ion mobility spectrometry, *Anal. Chem.*, 57, 1902, 1985.
68. **Levine, I. N.,** in *Physical Chemistry,* McGraw-Hill, New York, 1983, 467.
69. **Siegel, M. W.,** Atmospheric pressure ionization, in *Plasma Chromatography,* Carr, T. W., Ed., Plenum Press, New York, 1984, 95.
70. **Gray, D. E., Ed.,** *AIP Handbook,* McGraw-Hill, New York, 1972, 256.
71. **Poole, C. F. and Zlatkis, A.,** in *Electron Capture, Theory and Practice in Chromatography,* Elsevier/North-Holland, Amsterdam, 1981, 13.
72. **Weast, R. C., Ed.,** *CRC Handbook of Chemistry and Physics,* CRC Press, Boca Raton, FL, 1972, B-264.
73. **Pellizzari, E. D.,** Electron capture detection in gas chromatography, *J. Chromatogr.*, 98, 323, 1974.
74. **Eiceman, G. A., Leasure, C. S., Vandiver, V. J., and Rico, G.,** Flow characteristics in a segmented closed-tube design for ion mobility spectrometry, *Anal. Chim. Acta.*, 175, 135, 1985.
75. **Good, A., Dunder, D. A., and Kebarle, P.,** Ion-molecule reactions in pure nitrogen and nitrogen containing traces of water at total pressures 0.5—4 torr. Kinetics of clustering reactions forming $H^+(H_2O)n$, *J. Chem. Phys.*, 52, 212, 1970.
76. **Sumner, J., Nicol, G., and Kebarle, P.,** Sensitivity enhancements obtained at high temperatures in atmospheric pressure ionization mass spectrometry, *Anal. Chem.*, 60, 1300, 1988.
77. **Carroll, D. I., Dzidic, I., Stillwell, R. N., and Horning, E. C.,** Identification of positive reactant ions observed for nitrogen carrier gas in plasma chromatography mobility studies, *Anal. Chem.*, 47, 1956, 1975.
78. **Carr, T. W.,** Comparison of the negative reactant ions formed in the plasma chromatograph by nitrogen, air, and sulfur hexafluoride as the drift gas with air as the carrier gas, *Anal. Chem.*, 51, 705, 1979.
79. **Siegel, M. W. and Fite, W. L.,** Terminal ions in weak atmospheric pressure plasmas. Applications of API to trace impurity analysis in gases, *J. Phys. Chem.*, 80, 2871, 1976.
80. **Harrison, A. G.,** *Chemical Ionization Mass Spectrometry,* CRC Press, Boca Raton, FL, 1983.

81. **Kim, S. H. and Betty, K. R.,** Plasma chromatography of benzene with mass identified mobility spectra, *Anal. Chem.*, 50, 1784, 1978.
82. **Karasek, F. W., Kim, S. H., and Hill, H. H., Jr.,** Mass identified mobility spectra of p-nitrophenol and reactant ions in plasma chromatography, *Anal. Chem.*, 48, 1133, 1978.
83. **Karasek, F. W. and Kane, D. M.,** Ionic species of organic compounds observed in mobility spectra by plasma chromatography, *J. Chromatogr.*, 93, 125, 1974.
84. **Dressler, M.,** *Selective Gas Chromatographic Detectors*, Elsevier, New York, 1986, 217.
85. **Carr, T. W.,** Analysis of semiconductor devices and microelectronic packages by plasma chromatography mass spectrometry, in *Plasma Chromatography*, Plenum Press, New York, 1984, 215.
86. **Blyth, D. A.,** A vapor monitor for detection and contamination control, in Proc. Int. Symp. Against Chem. Warfare Agents, Stockholm, 1983.
87. **Franklin, J. L. and Harland, P. W.,** Gaseous negative ions, *Anal. Rev. Phys. Chem.*, 25, 485, 1974.
88. **Sevcik, J. and Krysl, S.,** A photoionization detector, *Chromatographia*, 6, 375, 1973.
89. **Serum, P. I.,** Quenching or enhancement of the response of the photoionization detector, *J. Chromatogr.*, 205, 413, 1981.
90. **Freedman, A. N.,** The photoionization detector. Theory, performance and application as a low-level monitor of oil vapour, *J. Chromatogr.*, 190, 263, 1980.
91. **Ostojic, N. and Sternberg, Z.,** A new photoionization detector for gas chromatography, *Chromatographia*, 7, 3, 1974.
92. **Norlander, B., Carlsson, B., and Bertler, A.,** Sensitive assay of methadone in plasma by using capillary gas chromatography with photoionization detection, *J. Chromatogr.*, 375, 313, 1986.
93. **Leasure, C. S., Fleischer, M. E., Anderson, G. K., and Eiceman, G. A.,** Photoionization in air with ion mobility spectrometry using a hydrogen discharge lamp, *Anal. Chem.*, 58, 2142, 1986.
94. **Lubman, D. M. and Kronick, M. N.,** Discrimination of isomers of xylene by resonance enhanced two-photon ionization, *Anal. Chem.*, 54, 1546, 1982.
95. **Lubman, D. M. and Kronick, M. L.,** Multiwavelength-selective ionization of organic compounds in an ion mobility spectrometer, *Anal. Chem.*, 55, 867, 1983.
96. **Eiceman, G. A., Vandiver, V. T., Leasure, C. S., Anderson, G. K., Tiee, T. T., and Danen, W. C.,** Effects of laser beam parameters in laser-ion mobility spectrometry, *Anal. Chem.*, 58, 1690, 1986.
97. **Patterson, P. L.,** Recent advances in thermionic ionization detection for gas chromatography, *J. Chromatogr. Sci.*, 24, 41, 1986.
98. **Vora, K. N., Campbell, D. N., Davis, R. C., Spangler, G. E., and Reategni, J. A.,** European Patent Appl. EP 198154 AZ, 22 October 1986.
99. **McMinn, D., Shumate, C., Hallen, R., Siems, W. F., and Hill, H. H., Jr.,** unpublished.
100. **Geniec, J., Mack, L. L., Nakamae, K., Gupta, C., Kumar, V., and Dole, M.,** Electrospray mass spectroscopy of macromolecules: application of an ion-drift spectrometer, *Biomed. Mass Spectrom.*, 11, 259, 1984.
101. **Shumate, C. B. and Hill, H. H., Jr.,** unpublished.
102. **Doyle, A., Moffett, D. R., and Vonnegut, B.,** Behavior of evaporating electrically charged droplets, *J. Colloid Sci.*, 19, 136, 1964.
103. **Yamashita, M. and Fenn, J. B.,** Electrospray ion source. Another variation on the free-jet theme, *J. Phys. Chem.*, 88, 4451, 1984.
104. **Dole, M., Gupta, C. V., Mack, L. L., and Nakamae, K.,** Application of the plasma chromatograph to polystyrene, *Polym. Prepr.*, 18, 188, 1977.
105. **Blanchard, W. C.,** Control of ion TOF increases performance of chemical sensor, *Res. Dev.*, August, 50, 1988.
106. **Baim, M. A., Schuetze, F. J., Frame, J. M., and Hill, H. H., Jr.,** A microprocessor-controlled ion mobility spectrometer for selective and nonselective detection following gas chromatography, *Am. Lab.*, 14, 59, 1987.
107. **Conrad, F. J.,** Explosives detection, the problem and prospects, *J. Inst. Nucl. Mater. Manage.*, 13, 212, 1984.
108. **Cohen, M. J., Wernlund, R. F., and Stimac, R. M.,** The ion mobility spectrometer for high explosive vapor detection, *J. Inst. Nucl. Mater. Manage.*, 13, 220, 1984.
109. **Lawrence, A. H. and Elias, L.,** Field screening techniques in forensic case work: trace evidence detection of organonitrate explosives and some illicit drugs, *ACS Symp. Anal. Methods Foren. Chem.*, Miami, FL, 1985.
110. **Lawrence, A. H. and Elias, L.,** Application of air sampling and ion mobility spectrometry to narcotics detection: a feasibility study, *U.N. Bull. Narc.*, 37, 1, 1985.
111. **Lawrence, A. H.,** Ion mobility spectrometry/mass spectrometry of some prescription and illicit drugs, *Anal. Chem.*, 58, 1269, 1986.
112. **Wernlund, R. F. and Cohen, M. T.,** Measuring trace levels of nickel carbonyl, *Res. Dev.*, 32, 1975.
113. **Watson, W. M. and Kohler, C. F.,** Continous environmental monitoring of nickel carbonyl by Fourier transform infra red spectrometry and plasma chromatography, *Environ. Sci. Technol.*, 13, 1241, 1979.
114. **Eiceman, G. A., Fleischer, M. E., and Leasure, C. S.,** Sensing of petrochemical fuels in soils using headspace analysis with photoionization-ion mobility spectrometry, *Int. J. Environ. Anal. Chem.*, 28, 279, 1987.
115. **Carr, T. W.,** Analysis of surface contaminents by plasma-chromatography/mass spectrometry, *Thin Solid Films*, 45, 115, 1977.
116. **Carr, T. W.,** Analysis of polymer outgassing as studied by plasma chromatography-mass spectrometry, *NBS Spec. Publ.*, 519, 697, 1979.
117. **Karasek, F. W. and Keller, R. A.,** Gas chromatograph/plasma chromatograph interface and its performance in the detection of musk ambrette, *J. Chromatogr. Sci.*, 10, 626, 1972.
118. **Ramstad, T., Nestrick, T. J., and Tou, J. C.,** Studies of the effects of volatile components from gas chromatographic liquid phases on plasma chromatographic performance, *J. Chromatogr. Sci.*, 16, 240, 1978.
119. **Baim, M. A. and Hill, H. H., Jr.,** Halogenated compound response in an oxygen doped ion mobility detector for capillary gas chromatography, *J. High Resolution Chromatogr. Chromatogr. Commun.*, 6, 4, 1983.
120. **Baim, M. A. and Hill, H. H., Jr.,** Determination of 2,4-dichlorophenoxyacetic acid in soils by capillary gas chromatography with ion-mobility detection, *J. Chromatogr.*, 279, 631, 1983.
121. **Eatherton, R. L., Siems, W. F., and Hill, H. H., Jr.,** Fourier transform ion mobility spectrometry of barbituates after capillary gas chromatography, *J. High Resolution Chromatogr. Chromatogr. Commun.*, 9, 44, 1986.
122. **St. Louis, R. H., Siems, W. F., and Hill, H. H., Jr.,** Evaluation of direct axial sample introduction for ion mobility detection after capillary gas chromatography, *J. Chromatogr.*, 479, 221, 1989.
123. **St. Louis, R. H., Siems, W. F., and Hill, H. H., Jr.,** Ion mobility detection after capillary gas chromatography, *LC/GC*, 9, 810, 1988.
124. **Lee, M. L., Yang, F. J., and Bartle, K. D.,** *Open Tubular Column Gas Chromatography, Theory and Practice*, Wiley-Interscience, New York, 1984, 129.
125. **Rokushika, S., Hatano, H., and Hill, H. H., Jr.,** Ion mobility spectrometry after supercritical fluid chromatography, *Anal. Chem.*, 59, 8, 1987.
126. **Eatherton, R. L., Morissey, M. A., Siems, W. F., and Hill, H. H., Jr.,** Ion mobility detection after supercritical fluid chromatography, *J. High Resolution Chromatogr. Chromatogr. Commun.*, 9, 154, 1986.
127. **Eatherton, R. L., Morrissey, M. A., and Hill, H. H., Jr.,** Com-

parison of ion mobility constants of selected drugs after capillary gas chromatography and capillary supercritical fluid chromatography, *Anal. Chem.*, 60, 2240, 1988.
128. **Tarver, E. and Hill, H. H., Jr.,** ECD-like response after supercritical fluid chromatography, West. ACS Conv., Los Angeles, 1988.
129. **Morrissey, M. M. and Hill, H. H., Jr.,** unpublished data.
130. **Hill, H. H., Jr. and Morrissey, M. A.,** Ion mobility spectrometry as a detection method for supercritical fluid chromatography, in *Modern Supercritical Fluid Chromatography,* White, C. M., Ed., Hüthig, Heidelberg, 1988, 95.
131. **Karasek, F. W. and Denny, D. W.,** Evaluation of the plasma chromatograph as a qualitative detector for liquid chromatography, *Anal. Lett.*, 6(11), 993, 1973.
132. **McMinn, D., Hallen, R., and Hill, H. H., Jr.,** unpublished data.